Identifying and Isolating a Flat Band in 2D Systems

Jun Hyung Bae

A Thesis
in
The Department
of
Physics

Presented in Partial Fulfillment of the Requirements
for the Degree of Master of Science (Physics) at
Concordia University
Montreal, Quebec, Canada

November 2020
©Jun Hyung Bae, 2020

CONCORDIA UNIVERSITY
School of Graduate Studies

This is to certify that the thesis prepared

By: Jun Hyung Bae

Entitled: Identifying and Isolating a Flat Band in 2D Systems

and submitted in partial fulfillment of the requirements for the degree of

Master of Science (Physics)

complies with the regulations of the University and meets the accepted standards with respect to originality and quality.

Signed by the final examining committee:

Gilles Peslherbe _____ Chair

Pablo Bianucci _____ Examiner

Panagiotis Vasilopoulos _____ Examiner

Saurabh Maiti _____ Thesis Supervisor(s)

_____ Thesis Supervisor(s)

Approved by _____

Valter Zazubovits Chair of Department or Graduate Program Director

Pascale Sicotte
Dean

Abstract

Identifying and Isolating a Flat Band in 2D Systems

Jun Hyung Bae

Flat band systems are gaining popularity due to special properties. For instance, the strong correlation of electrons in flat bands leads to realization of unconventional superconductivity. Typically, such bands are only approximately flat and are engineered by fine tuning Vanderwaal's structures. On the other hand, systems with perfectly flat bands provide a ground for studying exotic quasi-particles such as composite fermions in the fractional quantum Hall state. These flat bands, however, are induced by an external field. Here we explore other systems that host perfectly flat bands, namely the Kagome lattice and the Lieb lattice. One issue with these lattices, however, is that their flat bands are degenerate with other bands. This thesis will explore means to lift the degeneracy while preserving the flatness of the band. It will also demonstrate that the flatness is robust under certain modifications to the lattice and that, unlike suggested by past studies, breaking time-reversal symmetry is not sufficient to isolate the flat band. Instead, we will show that modulating the flux arising from a Chern-Simons type field gaps out the band without disturbing its flatness.

Acknowledgements

First and foremost I would like to thank God for having given me this opportunity to study and blessing me to meet wonderful people to provide me help and guidance. I would also like to thank my supervisor, Dr. Saurabh Maiti, for being such a great mentor. Not only he has a deep understanding and knowledge in the subject but also he has passion that motivates me. With his patience, he has trained me to think like a physicist. I must also thank a member of my research group, Igor Benek Lins, for always being so supportive and willing to help me. In particular, the presentation of this thesis improved a lot with his revision and the figures he prepared for me.

Contents

List of Figures

1 Introduction

Strongly correlated systems are useful for studying exotic systems such as fractional quantum Hall effect (FQHE) [1, 2], the Wigner crystal [3–5], unconventional superconductivity at near room temperature [6, 7], and Mott insulator [8, 9]. There are two ways that strong correlation effects can be induced in a lattice. One way is by having a high density of states. When the product of density of states at the Fermi surface and the Coulomb interactions is greater than 1, the correlation is considered strong. Another way is having a dominant contribution of potential energy due to Coulomb interactions over the kinetic energy to the total energy. Kinetic energy is proportional to the Fermi energy whose range is dependent on the associated bandwidth while the potential energy is governed by the Coulomb interactions. Kinetic energy can be quenched by having zero bandwidth in the system. The two scenarios of forming strong correlation effects can be observed in two different kinds of systems. The high-density-of-states scenario can be seen in a system with a dispersing (or approximately flat) band whose density of states is high while the zero-kinetic-energy scenario can be seen in a system with a perfectly flat band.

Twisted bilayer graphene is an example of a system that exhibits an approximately flat band with strong correlation effects. It is constructed by stacking two sheets of graphene on top of each other then twisting to the magic angle of 1.1° [10]. It is studied in a wide range of applications. [11–14]. There are, however, areas that can only be studied with systems with perfectly flat bands such as phenomena involving exotic quasiparticles. For example, Electronic correlations lead to the emergence of Chern-Simon's field that leads to the FQHE. The strong repulsive interaction due to quenching of the kinetic energy induces the localization of sites at a certain filling fraction of degenerate states (in the FB). The resulting configuration describes the Wigner crystal.

Due to these interesting applications, there are researchers who seek for methods to engineer (perfectly) flat band systems. The conventional method of generating a flat band system is mathematically challenging. It requires solving inverse eigenvalue problems, which is difficult to do and may not even have a solution in some cases. Often, these proposed flat band systems are only applicable for long-range hoppings. There is an alternative approach introduced by Xu and Pu of using Gram matrices [15]. This method, however, is limited only for a specific number of atoms per unit cell for a given spatial dimension. This is not very ideal in terms of practicality. In engineering real materials based on theoretical models, it is preferred that the hoppings are short-range for practicality purposes. One of the meaningful outcomes of this thesis is the realization of two families of readily constructible flat band systems with nearest-neighbour hoppings based on the Kagome and Lieb lattices.

Like most other flat band systems, the Kagome and Lieb lattices exhibit perfectly flat bands

that are degenerate with their adjacent dispersive bands. Degenerate flat bands are disadvantageous in studying the phenomena mentioned above. When a flat band is coupled to a dispersive band, the strong correlation effects are overshadowed by the dispersion. Thus, it is desirable to lift the degeneracy to take advantage of the flat band. Additionally, when the degeneracy is lifted, the topology of the flat band can be studied. Thus, it is worthwhile to explore means to lift degeneracies in flat band systems. A past study showed that the band touching is protected by the topological structure [16]. Furthermore, it was demonstrated that when time-reversal symmetry (TRS) is broken, flat bands are isolated (but it was also pointed out that there is no proof that breaking TRS is a necessary condition to isolate flat bands) [17]. One of the goals of this thesis is to show that breaking TRS is not sufficient to isolate and preserve flat bands in lattices like the Kagome lattice and present an appropriate treatment.

The thesis is constructed in the following order. Chapter 2 will introduce the two lattices that will be studied throughout the thesis; Kagome lattice and Lieb lattice. Their band structures will be presented by diagonalizing the Hamiltonians to show that both lattices exhibit a flat band. In addition, an analytical approach to calculating the energies of the flat bands will be presented. This analytical approach will also enable us to calculate the energies of the flat bands in modified lattices.

Chapter 3 will show that breaking TRS by applying an external magnetic field lifts the degeneracy but does not preserve the flat band in Kagome lattice. The presence of magnetic field will be reflected in the Hamiltonian by adding appropriate phases with the help of Peierl's substitution. By diagonalizing the Hamiltonians for different strengths of magnetic field Hofstadter's spectrum will be plotted, which will show the bandwidths and gaps of the energy bands at all possible values of magnetic field. The spectrum will reveal that the degeneracy is lifted but the flat band becomes dispersive as soon as the external magnetic field takes a non-zero value. On the other hand, applying an external magnetic field will be shown to be sufficient to isolate the flat band in the Lieb lattice. The Hofstadter's spectrum of the Lieb lattice will show that the flat band remains flat and the degeneracy is lifted in the presence of magnetic field. The reason for the two different results, the flat band not being preserved in the Kagome lattice and being preserved in the Lieb lattice, will be explained in Chapter 6.

In the mean time, Chapter 4 will focus on the degeneracy of the flat bands. Two methods of calculating degeneracy will be presented. The first method equates the eigenvalues associated with the flat bands to those of the dispersive bands with which they are degenerate. The second method presents mathematical constraints at the level of Hamiltonian. By applying these constraints to the Hamiltonian matrix, the associated degeneracies of the system can be identified. The constraints will be found for systems with 2,3, and 4 (identical) atoms per unit cell. As examples, Graphene and extended square lattice in addition to Kagome lattice and Lieb lattice

will be explored. The advantage of the first approach is that the calculation is relatively simple once the eigenvalues are found. On the other hand, the advantage of the second approach is that it does not require the calculation of eigenvalues.

Chapter 5 will discuss the robustness of flat bands, particularly, under lattice modifications. The purpose of this chapter is to demonstrate that flat band systems can exist for a family of systems and not just for fine-tuned set of parameters. Three realizable types of modifications will be considered, two will be shown to fail to preserve the flat bands while the third one succeed. To be specific, the unit cell of Kagome lattice is chosen to be a parallelogram whose four vertices together make up one atom, midpoints of two horizontal sides make up one atom, and midpoints of the slanted vertical sides make up one atom. The first type of modification is strains along the two diagonal axes of the unit cell. It will be shown that this fails to preserve the flat band. The second type of modification will make the three kinds of atoms in the lattice different from one another, which is reflected in the Hamiltonian as the three on-site energies having different values. The result will be similar to the first one in the sense that the flat band is not preserved. The last type of modification will group the inter-unit cell bonds and the intra-unit cell bonds separately and vary the ratio between the two groups, which corresponds to changing the distance between unit cells. The result will show that the flat band is preserved and remains unchanged while the dispersive bands go through changes as the ratio varies. This same type of modification will also be applied to the Lieb lattice whose unit cell is a square with the four vertices making up one atom and midpoints of each pair of facing sides making up one atom each. It will be shown that the flat band remains unchanged while the dispersive bands go through changes just like the case of Kagome lattice. This seeminglyl artificial modification, is readily achievable in optical lattices or photonic crystals. Our analytic treatment allows us to parametrize the two families of flat band systems.

Lastly, in chapter 6, the Chern-Simons (CS) field will be introduced. It will be shown that the presence of a CS field successfully isolates the flat band in the Kagome lattice, which was not the case when the magnetic field was applied. The main difference between the magnetic field and the CS field is the distribution of flux in the unit cell. Due to the presence of internal bonds in the unit cell of Kagome lattice, flux is distributed among three regions. Applying a magnetic field results in distributing the flux in all three regions proportionally to the respective areas. On the other hand, the presence of CS field causes the flux to be concentrated in one region such that the other two regions have zero flux. The effect of CS field on the flat band of Kagome lattice will be observed in the Hofstadter's spectrum. It will reveal that the flat band is preserved and it is gapped out for all possible values of flux per unit cell. Moreover, it will be discussed that due to the absence of internal structure in the unit cell of the Lieb lattice there is no difference in the distribution of flux between the magnetic field and the CS field, which

implies that the presence of CS field will isolate the flat band of Lieb lattice. To emphasize the effect of CS field that isolates flat bands, the family of Kagome lattices introduced in Chapter 5 will be examined. The result will confirm that the presence of CS field indeed isolates flat bands.

2 Flat Bands

Both Kagome lattice and Lieb lattice exhibit perfectly flat bands which are coupled to dispersive bands. Despite the fact that Kagome materials are relatively rare, the Kagome lattice has gained popularity and is widely studied particularly in relation to quantum spin liquid states [18, 19]. One example of Kagome material is Fe_3Sn_2 [20]. This is a 3D material that consists of a Kagome structure in one of its crystal planes. Furthermore, the Lieb lattice, with its unique electronic structure, features many interesting physical phenomena such as superconductivity and ferromagnetism [21, 22]. The Lieb lattice has been realized in optical lattices [23] . In addition, its material realization has been proposed with synthesized covalent-organic framework [24, 25].

The following sections will introduce the two lattices in more detail and analytically calculate their flat bands.

2.1 Kagome Lattice

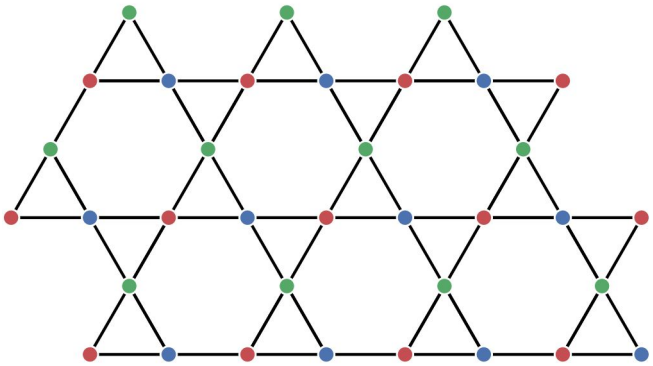

Figure 1: Kagome lattice structure; there are three atoms per unit cell.

Kagome lattice is composed of three atoms per unit cell as shown in Figure (1). With lattice constant 2a, the Hamiltonian can be written as following.

$$H = -t \begin{pmatrix} 0 & 1 + e^{iR_1 \cdot k} & 1 + e^{iR_2 \cdot k} \\ 1 + e^{-iR_1 \cdot k} & 0 & 1 + e^{iR_3 \cdot k} \\ 1 + e^{-iR_2 \cdot k} & 1 + e^{-iR_3 \cdot k} & 0 \end{pmatrix} \tag{2.1}$$

where $R_1 = (-2a, 0), R_2 = (-a, -\sqrt{3}a), R_3 = (a, -\sqrt{3}a)$ are the translation vectors and t is the hopping amplitude, which is the overlap integral between the two sites in consideration.

The Hamiltonian can be diagonalized to give three eigenvalues that make up the energy band structure as shown in Figure (2).

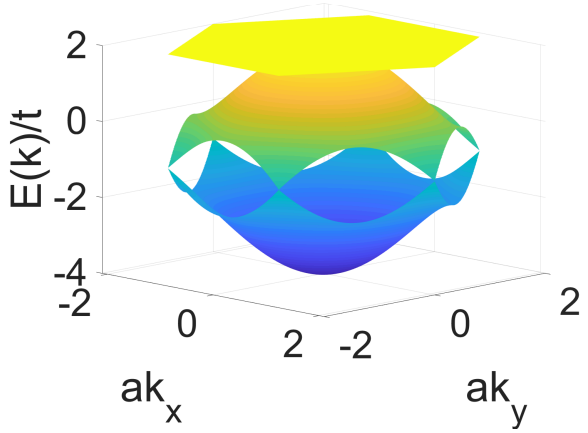

Figure 2: Energy band structure of Kagome lattice; the top band is dispersionless at $\frac{E}{t} = 2$.

Observe in the band structure that the top most band is flat at $\frac{E}{t} = 2$. This can be calculated analytically. By representing the Hamiltonian in the following form,

$$H = -t \begin{pmatrix} 0 & \alpha_2 & \alpha_1 \\ \alpha_2^* & 0 & \alpha_3 \\ \alpha_1^* & \alpha_3^* & 0 \end{pmatrix} \tag{2.2}$$

where $\alpha_i \equiv 1 + e^{iR_i \cdot k}$, the characteristic polynomial can be found as

$$|H - \lambda I| = \left(\frac{\lambda}{t}\right)^3 - \left(\frac{\lambda}{t}\right)\left(|\alpha_1|^2 + |\alpha_2|^2 + |\alpha_3|^2\right) + \alpha_1\alpha_2^*\alpha_3 + \alpha_1^*\alpha_2\alpha_3^* = 0 \tag{2.3}$$

Notice that the last two terms are conjugate to each other. Then, the sum can be expressed as $2Re[\alpha_1^*\alpha_2\alpha_3^*]$. Thus, the characteristic polynomial can be re-written as

$$\left(\frac{\lambda}{t}\right)^3 - \left(\frac{\lambda}{t}\right)\left(|\alpha_1|^2 + |\alpha_2|^2 + |\alpha_3|^2\right) + 2Re[\alpha_1^*\alpha_2\alpha_3^*] = 0 \tag{2.4}$$

Now, for a flat band to exist, one of the solutions of the characteristic equations must be constant (call it λ_c), independent of k. Define a new variable f in relation to the constant root $f \equiv \frac{\lambda_c}{t}$. Furthermore, to make the computations for finding the actual values of f easier,

perform a gauge transformation on the eigenvectors according to

$$(v_1, v_2, v_3) \rightarrow \left(v_1, e^{\frac{ikR_1}{2}} v_2, e^{\frac{ikR_2}{2}} v_3\right) \tag{2.5}$$

Then, the corresponding Hamiltonian is

$$H = -2t \begin{pmatrix} 0 & \cos(\frac{kR_1}{2}) & \cos(\frac{kR_2}{2}) \\ \cos(\frac{kR_1}{2}) & 0 & \cos(\frac{kR_3}{2}) \\ \cos(\frac{kR_2}{2}) & \cos(\frac{kR_3}{2}) & 0 \end{pmatrix} \tag{2.6}$$

Then, substitute the values of α's to get

$$|\alpha_1|^2 + |\alpha_2|^2 + |\alpha_3|^2 = 6 + 2\sum_{i=1}^{3} \cos(kR_i) \tag{2.7}$$

$$2Re[\alpha_1^* \alpha_2 \alpha_3^*] = 4 + 4\sum_{i=1}^{3} \cos(kR_i) \tag{2.8}$$

The characteristic polynomial in equation (2.4) becomes

$$f^3 - f(6 + 2\sum_{i=1}^{3} \cos(kR_i)) + 4 + 4\sum_{i=1}^{3} \cos(kR_i) = 0 \tag{2.9}$$

$$\Rightarrow (f-2)\left(f^2 + 2f - 2 - 2\sum_{i=1}^{3} \cos(kR_i)\right) = 0 \tag{2.10}$$

It can be easily verified that $f = 2$ (or $\lambda_c = 2t$) solves the above equation. This precisely corresponds to the flat band at $\frac{E}{t} = 2t$.

2.2 Lieb Lattice

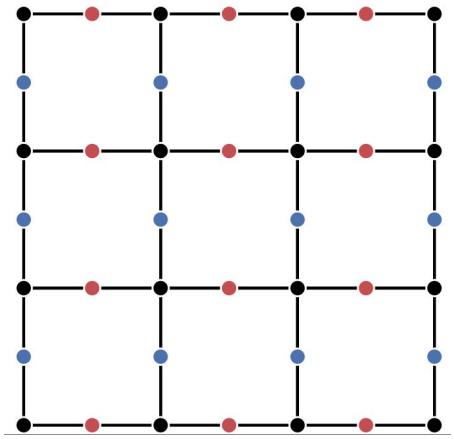

Figure 3: Lieb lattice structure; there are three atoms per unit cell.

Lieb lattice is another system composed of three atoms per unit cell. The Hamiltonian of a Lieb lattice with lattice constant $2a$ reads

$$H = -t \begin{pmatrix} 0 & 1+e^{ikR_1} & 1+e^{ikR_2} \\ 1+e^{-ikR_1} & 0 & 0 \\ 1+e^{-ikR_2} & 0 & 0 \end{pmatrix} \tag{2.11}$$

where $R_1 = (-2a, 0), R_2 = (0, -2a)$ are the translation vectors.

When the Hamiltonian is diagonalized, the band structure is plotted as shown in Figure (4).

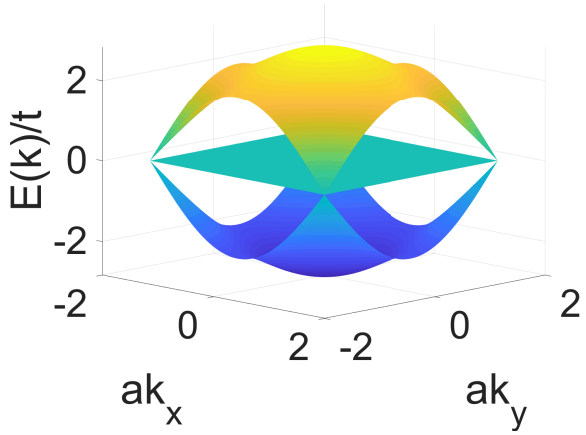

Figure 4: Lieb lattice energy dispersion; it has a flat band at $\frac{E}{t} = 0$.

Notice the flat band in the centre, $\frac{E}{t} = 0$. To have the analytical approach for this flat band,

first note that the Hamiltonian is of the following form.

$$-t \begin{pmatrix} 0 & \alpha_1 & \alpha_1 \\ \alpha_1^* & 0 & 0 \\ \alpha_2^* & 0 & 0 \end{pmatrix} \tag{2.12}$$

Then, the characteristic polynomial for the eigenvalues is

$$\left(\frac{\lambda}{t}\right)^3 - \left(|\alpha_1|^2 + |\alpha_2|^2\right)\left(\frac{\lambda}{t}\right) = 0 \tag{2.13}$$

The constant eigenvalue that corresponds to the flat band can be related to a new variable f again as $\lambda_c = ft$. Then, the characteristic polynomial can be expressed as

$$f(|\alpha_1|^2 + |\alpha_2|^2) = f^2 \tag{2.14}$$

It can be easily seen that $\lambda_c = 0$ solves the above equation. This agrees with the flat band at $\frac{E}{t} = 0$ in the band structure. There would have been another flat band if $|\alpha_1|^2 + |\alpha_2|^2$ were constant (independent of k), but $|\alpha_1|^2 + |\alpha_2|^2 = 4 + 2cos(ak_x) + 2cos(ak_y)$, which is clearly dependent on k.

3 Effect of Magnetic Field on Lattices

It has been demonstrated in a past study that when TRS is broken, degeneracy is lifted. This chapter will demonstrate that breaking TRS via applying external magnetic field not only lifts the degeneracy but also disperses the flatness. To begin, consider the usual (Maxwell-type) magnetic field directed perpendicular to the lattice plane. Let the field lie along the z-axis and the lattice plane on the x,y-plane. For simplicity, take Landau gauge for vector potential, $\vec{A} = B(0, x, 0)$. The choice of gauge makes calculations simpler due to the fact that the hopping amplitudes that are purely along the x-axis experience no effect by the vector potential. The presence of field is reflected in the Hamiltonian by adding phases to hopping amplitudes (that involve displacement along the y-direction) via Peierl's substitution. By diagonalizing the Hamiltonian constructed with the help of Peierl's substitution for a given value of magnetic field, the appropriate band structure can be calculated. Here, the magnetic field is represented by the number of flux quanta per unit cell, defined as ϕ.

Note that the purpose of diagonalizing Hamiltonians at various values of ϕ in this thesis is to examine what happens to the degeneracy and the flat band. In other words, the dispersion of the bands over the k-space is not significant as long as the bandwidths are shown. One tool that serves the goal perfectly is the Hofstadter's spectrum. Hofstadter's spectrum shows the bandwidths and gaps for all possible values of ϕ. More detailed presentation will follow in the subsequent sections.

3.1 External Magnetic Field on Kagome Lattice

In Kagome lattice, there is a total of six directions in which hoppings occur. In the presence of magnetic field, two hoppings among the six are along the horizontal axis and thus gain no new phase via Peierl's substitution. On the other hand, the remaining four require additional phases. They can be calculated as

$$
\begin{aligned}
2\pi\frac{e}{h}\int_{(ma,n\sqrt{3}a)}^{(ma+a,n\sqrt{3}a+\sqrt{3}a)} Bxdy &= \frac{\pi\phi}{4}\left(m+\frac{1}{2}\right)\\
2\pi\frac{e}{h}\int_{(ma,n\sqrt{3}a)}^{(ma+a,n\sqrt{3}a-\sqrt{3}a)} Bxdy &= -\frac{\pi\phi}{4}\left(m+\frac{1}{2}\right)\\
2\pi\frac{e}{h}\int_{(ma,n\sqrt{3}a)}^{(ma-a,n\sqrt{3}a-\sqrt{3}a)} Bxdy &= -\frac{\pi\phi}{4}\left(m-\frac{1}{2}\right)\\
2\pi\frac{e}{h}\int_{(ma,n\sqrt{3}a)}^{(ma-a,n\sqrt{3}a+\sqrt{3}a)} Bxdy &= \frac{\pi\phi}{4}\left(m-\frac{1}{2}\right)
\end{aligned}
$$

where m and n represent the displacement in the horizontal and vertical direction in unit of a (related to the lattice constant). The phases added to some of the hoppings are shown in Figure (5).

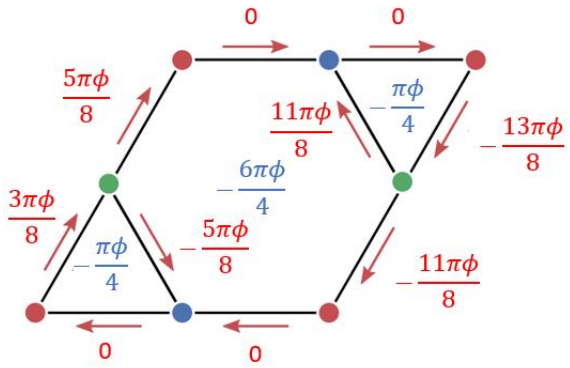

Figure 5: Phase assignment by Peierl's substitution; arrows indicate the direction of hopping and red texts correspond to the respective phases assigned via Peierl's substitution, blue texts indicate the flux through the region calculated by summing the phases along the edges.

With these new phases, the Hamiltonian can be properly constructed to reflect the presence of external field. By diagonalizing the Hamiltonians for different values of ϕ and taking the resultant bandwidths, the Hofstadter's spectrum can be in Figure (6) [26].

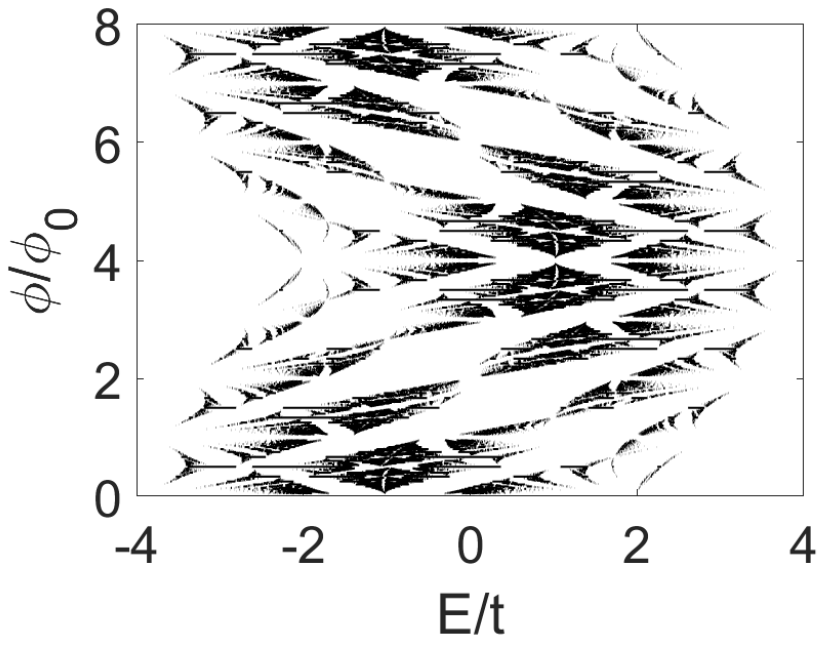

Figure 6: Hofstadter's spectrum of Kagome lattice; the flat band at $\phi = 0$ and $\frac{E}{t} = 2$ becomes dispersive (bandwidth grows) as ϕ grows.

In Figure (6), a horizontal line at a given ϕ represents the width of a band. The flat band at $\phi = 0$ (no magnetic field) and $\frac{E}{t} = 2$ begins to separate from its neighbouring dispersive band as ϕ grows. The white space between the top band (right-most bandwidth in the spectrum) its neighbouring band (immediately to the left of the right-most bandwidth in the spectrum) in the region approximately defined by $\frac{E}{t} \in [2, 2.5]$ and $\phi \in [0, 1]$ represents the gap between the two bands. This implies that the degeneracy is lifted. It should also be noticed that the top band gains finite width, which implies that the band is no longer flat. This clearly demonstrates that breaking TRS by applying external magnetic field removes the degeneracy but at the cost of dispersing the flat band. Furthermore, notice that ϕ ranges from 0 to 8. ϕ is periodic and the periodicity is due to the lattice structure. Kagome lattice has internal structure whose smallest region bounded by hoppings has a portion of the flux through the entire unit cell. The period of ϕ is determined by the number of this original unit cells needed to allow the smallest area to aquire a flux of 2π.

3.2 External Magnetic Field on Lieb Lattice

Lieb lattice involves four kinds of hoppings, where two are directed along the horizontal and thus gain no phase via Peierl's substitution. The other two are calculated as following.

$$2\pi\frac{e}{h}\int_{ma,na}^{ma,na+a} Bxdy = \frac{m\pi\phi}{2}$$
$$2\pi\frac{e}{h}\int_{ma,na}^{ma,na-a} Bxdy = -\frac{m\pi\phi}{2}$$

With these phases added to the Hamiltonian, the Hofstadter's spectrum can be plotted as shown in Figure (7) [27].

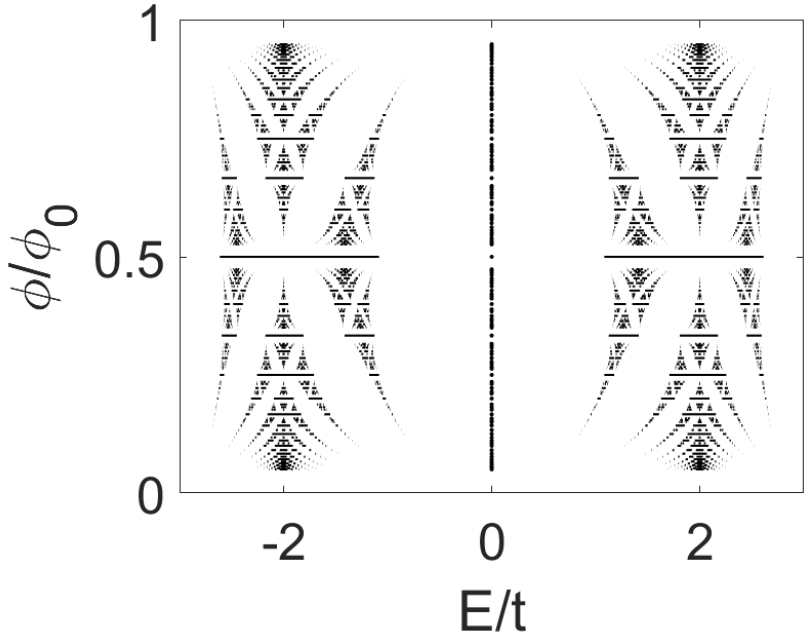

Figure 7: Hofstadter's spectrum of Lieb lattice; whenever band has zero width it is indicated with a point, it is shown that the flat band is preserved at $\frac{E}{t} = 0$ for all values of ϕ and also isolated.

Figure (7) is plotted by indicating with a dot whenever a band exists but its width is practically zero because otherwise the zero bandwidth would be reflected with white space in the plot. Thus, the thickness of the vertical line at $\frac{E}{t} = 0$ does not imply that the band has finite width but it is manually included there to make the flat band visible. It can be easily observed that this flat band is preserved and isolated from the two neighbouring dispersive bands for all values of $\phi \neq 0, 1$ (due to periodicity in ϕ, $\phi = 0$ is essentially identical to $\phi = 1$).

3.3 Summary

So far, it has been shown that applying an external magnetic field lifts the degeneracy in both Kagome lattice and Lieb lattice. There is, however, a difference between the two lattices. The flat band is not preserved in the Kagome lattice while it is preserved in the Lieb lattice. This will be explained further in Chapter 6 with the introduction of Chern-Simons field.

4 Degeneracy

Notice in both Kagome lattice and Lieb lattice in their band structures that both flat bands are coupled to dispersive bands as mentioned before. In order to lift the degeneracy, it is essential to understand what causes it and how to mathematically calculate it. The first part of this chapter will demonstrate how degeneracy can be computed in Kagome lattice and Lieb lattice. Latter part of the chapter will present a method to determine the existence of, and also to compute double and triple degeneracies for more general Hamiltonians. The method suggested is purely mathematical and it is not sufficient to provide a physical interpretation of the necessary criteria for the presence of degeneracy.

4.1 Calculation of Degeneracy by Equating Eigenvalues

4.1.1 (Double) Degeneracy in Kagome Lattice

It was found in Chapter 2.1 that the flat band of Kagome lattice is present at $\frac{E}{t} = 2$. One way to find the touching point of the flat band with its neighbouring dispersive band is to equate the two corresponding eigenvalues and compute the k point where the two are identical. In order to do this, the eigenvalue of the dispersive band must be calculated first.
Consider the characteristic polynomial in equation (2.4). Given one root $f = \frac{\lambda_c}{t}$, the polynomial can be factored by $\left(\frac{\lambda}{t} - f\right)$. In other words, the characteristic polynomial can be written in the following manner.

$$\left(\frac{\lambda}{t} - f\right)\left[\left(\frac{\lambda}{t}\right)^2 + f\left(\frac{\lambda}{t}\right) + f^2 - \left(|\alpha_1|^2 + |\alpha_2|^2 + |\alpha_3|^2\right)\right] = 0 \tag{4.1}$$

This allows the other two roots to be calculated as

$$\frac{\lambda_\pm}{t} = \frac{-f \pm \sqrt{4\left(|\alpha_1|^2 + |\alpha_2|^2 + |\alpha_3|^2\right) - 3f^2}}{2} \tag{4.2}$$

Again, for the double degeneracy to occur, the constant eigenvalue must be equated to one of the two dispersive roots. In other words,

$$\begin{aligned} f = \frac{\lambda_\pm}{t} &= \frac{-f \pm \sqrt{4\left(|\alpha_1|^2 + |\alpha_2|^2 + |\alpha_3|^2\right) - 3f^2}}{2} \\ &\Rightarrow 3f^2 = |\alpha_1|^2 + |\alpha_2|^2 + |\alpha_3|^2 \end{aligned} \tag{4.3}$$

Now, substituting the appropriate values for $\alpha_1, \alpha_2, \alpha_3$ according to the Hamiltonian of Kagome lattice as well as $f = 2$ gives

$$12 = 6 + 2\sum_{i=1}^{3} \cos(kR_i) \tag{4.4}$$

$$\Rightarrow 3 = \sum_{i=1}^{3} \cos(kR_i) \tag{4.5}$$

The above equality only holds for $\vec{k} = (0, 0)$. Referring to the band structure in Figure (2), it can be confirmed that the double degeneracy is in fact present at $\vec{k} = (0, 0)$.

4.1.2 (Triple) Degeneracy in Lieb Lattice

Same procedure is followed with the Lieb Lattice. Using the characteristic polynomial, in equation (2.13), found in the previous chapter, the remaining two roots can be found as

$$\frac{\lambda_{\pm}}{t} = \frac{-f \pm \sqrt{4\left(|\alpha_1|^2 + |\alpha_2|^2\right) - 3f^2}}{2} \tag{4.6}$$

To have the triple degeneracy as seen in the band structure, the constant root must be equated to the other two roots. After a simple rearrangement, the condition for the triple degeneracy is written as

$$3f^2 = |\alpha_1|^2 + |\alpha_2|^2 \tag{4.7}$$

Substituting the appropriate values for α_1, α_2 from the Hamiltonian and $f = 0$ gives

$$0 = cos^2(k_x) + cos^2(k_y) \tag{4.8}$$

Since both cosine terms are squared, the only time that the sum is zero is when they are both zero. This implies that both k_x and k_y are equal to $\pm\frac{\pi}{2}$. By observing the band structure it is also verified that at the four k points indicated, the flat band manifests triple degeneracy.
So far, by calculating the eigenvalues analytically and equating the appropriate eigenvalues with the one that corresponds to the flat band, it was demonstrated that degeneracy can be computationally found. The following sections discuss an alternative approach to calculating degeneracy in a more general manner, without having to cmopute eigenvalues.

4.2 Alternative Method of Calculating Degeneracy

Imagine an N-by-N Hamiltonian with N eigenvalues. The Schrodinger's equation writes $H_{N\times N}v_{N\times 1} = \lambda v_{N\times 1}$. The eigenstate has N number of unknowns given that the Hamiltonian has N number of equations. Normalization of v allows us to determine one of the unknowns and thus the system can have at most $N-1$ independent equations. Now, ssume two eigenvalues are identical, in other words there is double degeneracy. Let the two eigenvectors associated with the repeated eigenvalue be denoted as v_1 and v_2. Then, $H(v_1+v_2) = Hv_1 + Hv_2 = \lambda v_1 + \lambda v_2 = \lambda(v_1+v_2)$. It can be easily seen that any linear combination of the v_1 and v_2 is an eigenvector with the same eigenvalue. Denote an arbitrary linear combination as v. Then, $v = c_1v_1 + c_2v_2 = c_1\left(v_1 + \frac{c_1}{c_2}v_2\right)$. Here, c_1 is an overall scale and $\frac{c_1}{c_2}$ is unknown. In other words, one additional unknown parameter is introduced to the problem. Thus, only $N-2$ out of $N-1$ unknown variables can be determined. This necessarily requires $N-2$ linearly independent equations. Conversely, if the Hamiltonian has $N-2$ independent equations it means that there is double degeneracy. This same argument applies to any degree of degeneracy. For triple degeneracy, the Hamiltonian would have $N-3$ independent equations. Therefore, a relation between the degree of freedom and the number of independent equations can be defined.

$$\text{Rank of Hamiltonian} - \text{number of independent equations} = \text{degree of degeneracy} \tag{4.9}$$

Thus, if a system contains $N-1$ independent equations, there is no degeneracy and the situation corresponds to all the portion of the band structure except the degenerate points. This is possible because one additional equation is provided from the normalization to determine the eigenvector. For a similar reason, if all the equations in the system are independent, it is not solvable.

The following sections in this chapter will discuss the scheme to define conditions that bear degeneracy in systems of 2,3, and 4 atoms per unit cell (Hamiltonians of dimension 2,3, and 4). Applying the rule found for each size of Hamiltonian, double and triple degeneracies in Graphene, Kagome lattice, Lieb lattice, and extended square lattice will be mathematically derived.

4.2.1 Double Degeneracy in Hamiltonian of Rank 3

Consider a 3-by-3 Hamiltonian with identical atoms in the unit cell.

$$\begin{pmatrix} 0 & H_{12} & H_{13} \\ H_{21} & 0 & H_{23} \\ H_{31} & H_{32} & 0 \end{pmatrix} \begin{pmatrix} a \\ b \\ c \end{pmatrix} = E \begin{pmatrix} a \\ b \\ c \end{pmatrix} \tag{4.10}$$

$$\Rightarrow \begin{cases} H_{12}b + H_{13}c - Ea = 0 \\ H_{21}a + H_{23}c - Eb = 0 \\ H_{31}a + H_{32}b - Ec = 0 \end{cases} \tag{4.11}$$

Based on the relation between the degree of degeneracy and number of independent equations, it can be seen that double degeneracy occurs when there is one independent equation in rank-3 Hamiltonian (number of independent equation = 3 (rank) - 2 (double degeneracy)). It implies that all three equations are identical and they can simply be expressed as a scalar multiple of one another. In other words, the ratios of coefficients must be equal.

$$\begin{aligned} -\frac{E}{H_{21}} = -\frac{H_{12}}{E} = \frac{H_{13}}{H_{23}} \\ -\frac{E}{H_{31}} = \frac{H_{12}}{H_{32}} = -\frac{H_{13}}{E} \end{aligned} \tag{4.12}$$

One form of Hamiltonian that meets the above conditions is

$$\begin{pmatrix} 0 & -E & -E \\ -E & 0 & -E \\ -E & -E & 0 \end{pmatrix} \begin{pmatrix} a \\ b \\ c \end{pmatrix} = E \begin{pmatrix} a \\ b \\ c \end{pmatrix} \tag{4.13}$$

The above form of Hamiltonian corresponds to a situation where all the nearest-neighbour (NN) hopping amplitudes are identical among the three atoms and also that they are equal to the on-site energies. Thus for a system with double degeneracy for some k in the FBZ, its Hamiltonian can be reduced to (4.13).

4.2.2 Triple Degeneracy in Hamiltonian of Rank 3

For a rank-3 Hamiltonian to have triple degeneracy, the difference between the rank and the number of independent equations in the Hamiltonian has to be 3. In other words, there remains zero equation in this case. Then the Hamiltonian has to be a zero matrix, which gives zero

energy as well.

$$\begin{pmatrix} 0 & 0 & 0 \\ 0 & 0 & 0 \\ 0 & 0 & 0 \end{pmatrix} \begin{pmatrix} a \\ b \\ c \end{pmatrix} = 0 \begin{pmatrix} a \\ b \\ c \end{pmatrix} \tag{4.14}$$

This implies that all the NN hopping amplitudes and on-site energies are made zero and the triple degeneracy occurs at $\frac{E}{t} = 0$.

4.2.3 Example: Kagome Lattice

As an example of system with rank-3 Hamiltonian (lattice consists of three atoms per unit cell), consider Kagome lattice. The associated Hamiltonian is provided in section 2.1. The Hamiltonian can be tested for a double degeneracy by comparing it to the form in equation (4.13). It can be immediately realized that at $\frac{E}{t} = 2$ and $\vec{k} = 0$ (Γ point), double degeneracy occurs. Furthermore, by substituting appropriate values in condition (4.12), other places where double degeneracy occurs can be computed.

$$\begin{aligned} |H_{12}|^2 &= |H_{13}|^2 \\ \Rightarrow \cos(2k_x) - \cos(k_x - \sqrt{3}k_y) &= 0 \\ \Rightarrow -2sin\left(\frac{3k_x - \sqrt{3}k_y}{2}\right) sin\left(\frac{k_x + \sqrt{3}k_y}{2}\right) &= 0 \\ \Rightarrow 3k_x - \sqrt{3}k_y = 2n_1\pi \quad or \quad k_x + \sqrt{3}k_y &= 2n_2\pi \end{aligned} \tag{4.15}$$

$$\tag{4.16}$$

$$\begin{aligned} |H_{13}|^2 &= |H_{23}|^2 \\ \Rightarrow \cos(k_x - \sqrt{3}k_y) - \cos(k_x + \sqrt{3}k_y) &= 0 \\ \Rightarrow 2sin(k_x)sin(\sqrt{3}k_y) &= 0 \\ \Rightarrow k_x = n_3\pi \quad or \quad -\sqrt{3}k_y &= n_4\pi \end{aligned} \tag{4.17}$$

$$\tag{4.18}$$

$$\begin{aligned} |H_{12,13,23}|^2 &= E^2 \\ \Rightarrow 2 + 2\cos(2k_x) = 2 + 2\cos(k_x + \sqrt{3}k_y) &= 2 + 2\cos(2k_x - \sqrt{3}k_y) = E^2 \end{aligned} \tag{4.19}$$

where $n_1, n_2, n_3, n_4 \in \mathbb{Z}$.
The last constraint does not impose any restrictions on the value of $\vec{k}$ but it simply identifies the

value of $\frac{E}{t}$. Then, by combining the first two results, double degeneracy can be identified at

$$k_x = \frac{n\pi}{3}, \quad k_y = \frac{n\pi}{\sqrt{3}}$$

where $n \in \mathbb{Z}$.
This precisely coincides with the vertices of the FBZ (K/K' points) and E = -1.
The results of the calculations above can be compared to the band structure obtained by diagonalization in Figure (2). According to the figure, the top two bands are degenerate at $\vec{k} = (0, 0)$ and $\frac{E}{t} = 2$. The bottom two bands have six degenerate points at the vertices of the FBZ, which are

$$\vec{k} = \left(\frac{2\pi}{3}, 0\right), \left(\frac{\pi}{3}, \frac{\pi}{\sqrt{3}}\right), \left(-\frac{\pi}{3}, \frac{\pi}{\sqrt{3}}\right), \left(-\frac{2\pi}{3}, 0\right), \left(-\frac{\pi}{3}, -\frac{\pi}{\sqrt{3}}\right), \left(\frac{\pi}{3}, -\frac{\pi}{\sqrt{3}}\right)$$

Thus, the analytical calculations agrees with the result obtained via diagonalization.
Furthermore, the condition for triple degeneracy, equation (4.14), requires all the entries of the Hamiltonian to be zero, which cannot be achieved. To see this, equate H_{12} and H_{13} to zero.

$$1 + e^{-i2k_x} = 0 \Rightarrow k_x = -\frac{\pi}{2} \tag{4.20}$$

$$1 + e^{-i\left(-\frac{\pi}{2}\right) - i\sqrt{3}k_y} = 0 \Rightarrow k_y = -\frac{\pi}{2\sqrt{3}} \tag{4.21}$$

Now, since all elements have to be zero simultaneously, substitute these values in H_{23} and test if it can be equated to zero as well.

$$H_{23}\left(-\frac{\pi}{2}, -\frac{\pi}{2\sqrt{3}}\right) = 1 + e^{i\left(-\frac{\pi}{2}\right) - i\left(-\frac{\pi}{2\sqrt{3}}\right)} \tag{4.22}$$

This cannot be zero. Thus, there is no triple degeneracy in Kagome lattice.

4.2.4 Example: Lieb Lattice

Lieb lattice is another example of a system with rank-3 Hamiltonian. Refer to the Hamiltonian in section 2.2. The triple degeneracy can be tested by using equation (4.14). Recall that the Hamiltonian of Kagome lattice could not be made zero. But in the case of Lieb lattice, it is possible by substituting appropriate values for $\vec{k}$. In fact, the vertices of FBZ (K points, $\vec{k} = \left(\pm\frac{\pi}{2}, \pm\frac{\pi}{2}\right)$) make the Hamiltonian zero and the energy zero.
To test the existence of double degeneracy, substitute appropriate values in equation (4.13).

$$|1 + e^{-i2k_x}|^2 = |1 + e^{-i2k_y}|^2 = 0 = E^2 \tag{4.23}$$

Therefore,

$$|1 + e^{-i2k_x}|^2 = 0 \Rightarrow k_x = \pm\frac{\pi}{2} \tag{4.24}$$

$$|1 + e^{-i2k_y}|^2 = 0 \Rightarrow k_y = \pm\frac{\pi}{2} \tag{4.25}$$

Thus at $\vec{k} = \left(\pm\frac{\pi}{2}, \pm\frac{\pi}{2}\right)$, double degeneracy is present with energy 0. But this is precisely where the triple degeneracy is found. This is expected because a lower-degree degeneracy is a subspace of a higher-degree degeneracy. These results agree with the band structure plotted by diagonalizing the Hamiltonian in Figure (4).

4.2.5 Double Degeneracy in Hamiltonian of Rank 2

Whenever zero independent equations are assumed in a Hamiltonian of any rank, the Hamiltonian and the energy must be zero. Thus, in the case of double degeneracy in rank-2 Hamiltonians, the following must hold.

$$\begin{pmatrix} 0 & 0 \\ 0 & 0 \end{pmatrix} \begin{pmatrix} a \\ b \end{pmatrix} = 0 \begin{pmatrix} a \\ b \end{pmatrix} \tag{4.26}$$

Again, this corresponds to a situation where all NN hopping amplitudes and on-site energies are zero and thus results in double degeneracy at $\frac{E}{t} = 0$.

4.2.6 Example: Graphene

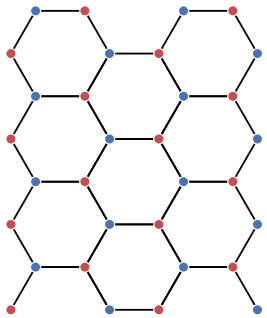

Figure 8: Graphene lattice; there are two atoms per unit cell.

Graphene is a popular example of system with rank-2 Hamiltonian. The lattice structure can be visualized in Figure (8). Consider the Hamiltonian of Graphene.

$$\begin{pmatrix} 0 & 1+e^{-i\frac{3}{2}ak_x+i\frac{\sqrt{3}}{2}ak_y}+e^{-i\frac{3}{2}ak_x-i\frac{\sqrt{3}}{2}ak_y} \\ 1+e^{i\frac{3}{2}ak_x-i\frac{\sqrt{3}}{2}ak_y}+e^{i\frac{3}{2}ak_x+i\frac{\sqrt{3}}{2}ak_y} & 0 \end{pmatrix} \tag{4.27}$$

Notice that the Hamiltonian becomes zero at the vertices of FBZ (K/K' points),

$$\vec{k} = \left(0, \frac{4\pi}{3\sqrt{3}}\right), \left(\frac{2\pi}{3}, \frac{2\pi}{3\sqrt{3}}\right), \left(\frac{2\pi}{3}, -\frac{2\pi}{3\sqrt{3}}\right), \left(0, -\frac{4\pi}{3\sqrt{3}}\right), \left(-\frac{2\pi}{3}, -\frac{2\pi}{3\sqrt{3}}\right), \left(-\frac{2\pi}{3}, \frac{2\pi}{3\sqrt{3}}\right)$$

Observe in Figure (9) that the six vertices of FBZ are doubly degenerate as predicted.

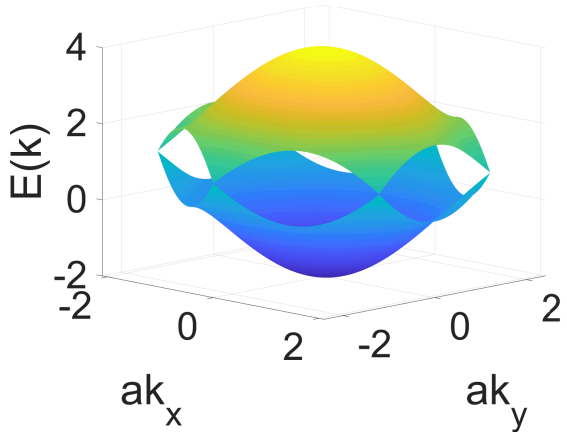

Figure 9: Energy dispersion of Graphene; notice the double degeneracy at the K/K' points.

4.2.7 Double Degeneracy in Hamiltonian of Rank 4

Consider a general 4-by-4 Hamiltonian (with identical atoms in the unit cell).

$$\begin{pmatrix} 0 & H_{12} & H_{13} & H_{14} \\ H_{21} & 0 & H_{23} & H_{24} \\ H_{31} & H_{32} & 0 & H_{34} \\ H_{41} & H_{42} & H_{43} & 0 \end{pmatrix} \begin{pmatrix} a \\ b \\ c \\ d \end{pmatrix} = E \begin{pmatrix} a \\ b \\ c \\ d \end{pmatrix} \tag{4.28}$$

$$\Rightarrow \begin{cases} H_{12}b + H_{13}c + H_{14}d = Ea \\ H_{21}a + H_{23}c + H_{24}d = Eb \\ H_{31}a + H_{32}b + H_{34}d = Ec \\ H_{41}a + H_{42}b + H_{43}c = Ed \end{cases} \tag{4.29}$$

Assume now that there are two linearly independent equations so that the system manifests double degeneracy. Without loss of generality, let the first and third equations be identical as well as the second and the fourth.

$$H_{12}b + H_{13}c + H_{14}d = Ea \Leftrightarrow H_{31}a + H_{32}b + H_{34}d = Ec \tag{4.30}$$

$$H_{21}a + H_{23}c + H_{24}d = Eb \Leftrightarrow H_{41}a + H_{42}b + H_{43}c = Ed \tag{4.31}$$

To make the two equations in each pair identical, the ratio of the coefficients of a,b,c,d must be set equal. In other words,

$$\begin{aligned} -\frac{E}{H_{31}} = \frac{H_{12}}{H_{32}} = -\frac{H_{13}}{E} = \frac{H_{14}}{H_{34}} \\ \frac{H_{21}}{H_{41}} = -\frac{E}{H_{42}} = \frac{H_{23}}{H_{43}} = -\frac{H_{24}}{E} \end{aligned} \tag{4.32}$$

Thus, when these conditions are satisfied for some k in the FBZ, the system has double degeneracy.

4.2.8 Triple Degeneracy in Hamiltonian of Rank 4

For a rank-4 Hamiltonian to have triple degeneracy, it has to be in the following form, where all the off-diagonal elements are equal to $-E$.

$$\begin{pmatrix} 0 & -E & -E & -E \\ -E & 0 & -E & -E \\ -E & -E & 0 & -E \\ -E & -E & -E & 0 \end{pmatrix} \tag{4.33}$$

This corresponds to a situation where all the on-site energies and NN hopping amplitudes are made equal to $\frac{E}{t}$, the energy at which the degeneracy takes place.

4.2.9 Example: Extended Square Lattice

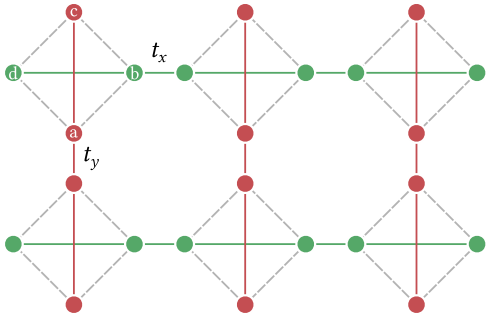

Figure 10: Extended square lattice; there are four atoms per unit cell and hopping amplitudes are allowed to vary.

An example of system with rank-4 Hamiltonian can be pictured with the basis of square lattice. While removing the atoms at the lattice sites, place four atoms at equidistance in the four directions along the horizontal and the vertical. Refer to Figure (10) for the lattice structure. the shortest hoppings amongst the four atoms, which are marked by the dashed lines in the figure, are defined as t_l. The hoppings in the vertical, or y direction, are indexed with subscript y. In addition, when the hopping is within the unit cell, it is given an additional superscript index in while for the hopping outside the unit cell it is indexed out. Same argument goes for the horizontal hoppings (x direction). The Hamiltonian of such system is given as

$$\begin{pmatrix} 0 & t_l & t_y^{in} + t_y^{out} e^{-i\vec{k}\cdot\vec{a}_2} & t_l \\ t_l & 0 & t_l & t_x^{in} + t_x^{out} e^{i\vec{k}\cdot\vec{a}_1} \\ t_y^{in} + t_y^{out} e^{i\vec{k}\cdot\vec{a}_2} & t_l & 0 & t_l \\ t_l & t_x^{in} + t_x^{out} e^{-i\vec{k}\cdot\vec{a}_1} & t_l & 0 \end{pmatrix} \tag{4.34}$$

Notice $H_{12} = H_{32}, H_{14} = H_{34}, H_{21} = H_{41}, H_{23} = H_{43}$. This means that the equations in (4.32) reduce to

$$-E = H_{31}, \quad -E = H_{24} \tag{4.35}$$

These conditions imply that $e^{i\vec{k}\cdot\vec{a}_1}$ and $e^{i\vec{k}\cdot\vec{a}_2}$ have to be real and the only way that they can be real is when

$$\vec{k} = (0,0), (\pm\pi, \pm\pi), (0, \pm\pi), (\pm\pi, 0) \tag{4.36}$$

Double degeneracy can only occur at the above k points. In particular, degeneracy at $\vec{k} = (0, \pm\pi), (\pm\pi, 0)$ can only be achieved when $t_y^{in} + t_y^{out} = t_x^{in} - t_x^{out}$ or $t_y^{in} - t_y^{out} = t_x^{in} - t_x^{out}$.

When these equalities do not hold, degeneracy may occur at the other k points.
To examine the existence of triple degeneracy, consider the form of Hamiltonian in equation (4.33). All the off-diagonal entries of the Hamiltonian must be equal to one another and to $-E$.

$$e^{-i\vec{k}\cdot\vec{a}_2} = e^{i\vec{k}\cdot\vec{a}_2} \Rightarrow \vec{k} = (0,0), (\pm\pi, \pm\pi) \tag{4.37}$$

$$t_l = t_y^{in} + t_y^{out} = t_x^{in} + t_x^{out} \tag{4.38}$$

This means that under the condition that the last line holds true, the k points in the first line are triply degenerate.

The results drawn above can be verified by substituting numerical values in the hopping parameters. To begin, factor out t_l in the Hamiltonian so that the new t_y's and t_x's are those of the original divided by t_l. Then, substitute $\vec{a}_1 = (1,0)$ and $\vec{a}_2 = (0,1)$.

$$H = \frac{1}{t_l}\begin{pmatrix} 0 & 1 & t_y^{in} + t_y^{out}e^{-ik_y} & 1 \\ 1 & 0 & 1 & t_x^{in} + t_x^{out}e^{ik_x} \\ t_y^{in} + t_y^{out}e^{ik_y} & 1 & 0 & 1 \\ 1 & t_x^{in} + t_x^{out}e^{-ik_x} & 1 & 0 \end{pmatrix} \tag{4.39}$$

As the first example, set all the hoppings to unity.

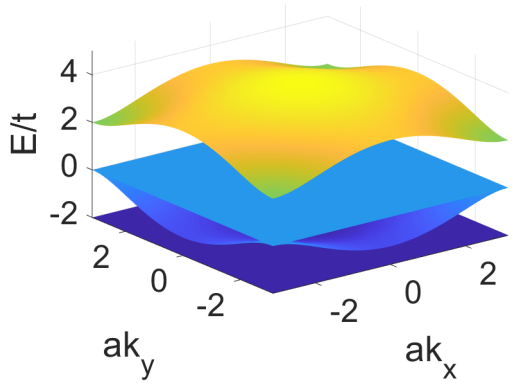

Figure 11: $t_x^{in} = 1, t_x^{out} = 1, t_y^{in} = 1, t_y^{out} = 1$; the three lowest bands are pair-wise doubly degenerate.

Notice that the condition for the degeneracy at $\vec{k} = (0, \pm\pi), (\pm\pi, 0)$ is not satisfied. Double degeneracy is present at $\vec{k} = (\pm\pi, \pm\pi)$ and the corresponding energy can be obtained as the negative of element $H_{13} = 0$. Moreover, the degeneracy at $(0,0)$ gives energy -2 based on the same reasoning.

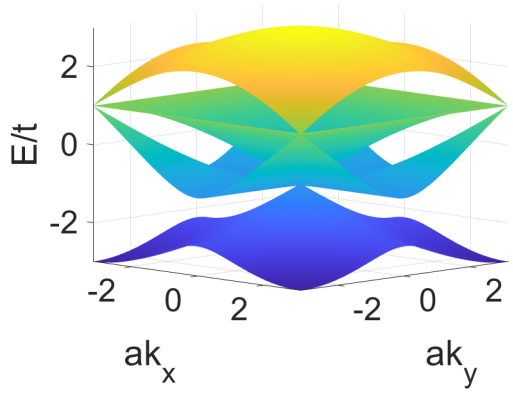

Figure 12: $t_x^{in} = 0, t_x^{out} = 1, t_y^{in} = 0, t_y^{out} = 1$; the upper three bands are triply degenerate at the vertices of BZ and also the lower three bands are triply degenerate at the centre.

As a second example, set the hoppings inside the square loop to zero. The condition for degeneracy at $\vec{k} = (0, \pm\pi), (\pm\pi, 0)$ is still not satisfied and thus there are no degeneracy at these points. But the degeneracy at $\vec{k} = (\pm\pi, \pm\pi)$ is present with energy 1. Also, the condition for triple degeneracy holds true exactly at $\vec{k} = (0, 0), (\pm\pi, \pm\pi)$ and it can be observed in the figure.

Lastly, to observe degeneracy at $\vec{k} = (0, \pm\pi), (\pm\pi, 0)$, let, for example, $t_y^{in} + t_y^{out} + t_x^{out} = t_x^{in}$ by setting all the terms on the left hand side 1 and the right hand side 3 so that there is degeneracy at $\vec{k} = (0, \pm\pi)$.

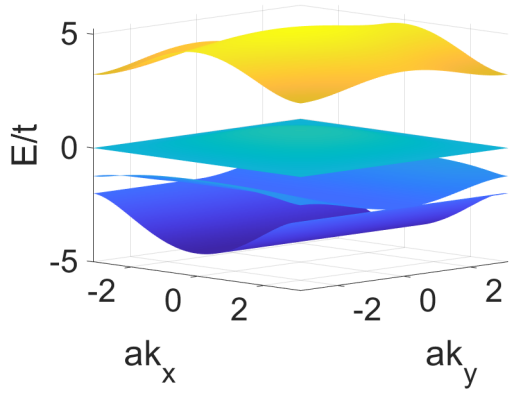

Figure 13: $t_x^{in} = 3, t_x^{out} = 1, t_y^{in} = 1, t_y^{out} = 1$; the bottom two bands are degenerate at points along the edges of BZ.

As demonstrated in this section, the system can be manipulated to manifest different degrees of degeneracy.

4.3 Summary

This chapter demonstrated two approaches for calculating degeneracy. The former of which requires calculating the eigenvalues and equating them while the latter compares the elements of Hamiltonian with the conditions found for each rank. The former is more advantageous for systems whose eigenvalues can be calculated easily but otherwise, the latter can be more useful. We will demonstrate the consistency of these findings with result in subsequent chapters.

5 Modified Lattices

This chapter is designed to examine the robustness of flat bands. To be specific, the Hamiltonian of Kagome lattice will be modified in three realizable ways. These are realizable because they will only consist of nearst neighbour hoppings. The first modification mimics applying strains along the two diagonal axes of the unit cell. The second modification requires making the three types atoms different from one another, which will result in different on-site energies in the Hamiltonian. The last modification requires varying the ratio between the hopping amplitudes within the unit cells and those outside the unit cells (between unit cells). It will be shown that only the last modification preserves the flat band and thus more suitable to the purpose of this thesis. Furthermore, real materials of this sort of modification can be fabricated with artificial growth techniques and also with nano-wires. Similarly for the Lieb lattice, the Hamiltonian will be modified with the different intra-unit-cell and inter-unit-cell hopping amplitudes. Moreover, an additional hopping amplitude will be considered to verify its effect on the flat band.

5.1 Applying Strains in Kagome Lattice

We consider two types of strains in Kagome lattice. They correspond to stretching the unit cell in the two diagonal directions. As it is described in Figure (14), in both cases the hopping amplitudes along the edges of the unit cell are reduced due to the increase in the distance. In the first case, where the stretching is applied to the longer diagonal of the unit cell, the internal hopping amplitudes grow in the process. On the other hand, the internal hopping amplitudes are reduced in the second case.

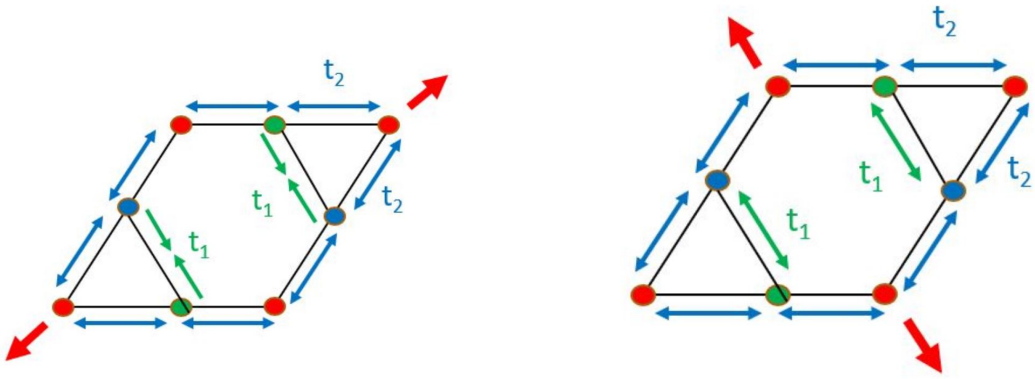

(a) $r \geq 1$ (b) $r < 1$

Figure 14: Two types of strains on Kagome lattice; the hopping amplitudes along the edges of the unit cell are defined as t_2 and those along the internal bonds are defined as t_1.

In both cases, the hopping amplitudes along the edges of the unit cell will be called t_2 and the internal hopping amplitudes t_1. Defining the ratio between the two $r = \frac{t_1}{t_2}$, the Hamiltonian can be written as

$$H = -t_2 \begin{pmatrix} 0 & 1 + e^{-i2ak_x} & 1 + e^{-iak_x - i\sqrt{3}ak_y} \\ 1 + e^{i2ak_x} & 0 & r + re^{iak_x - i\sqrt{3}ak_y} \\ 1 + e^{iak_x + i\sqrt{3}ak_y} & r + re^{-iak_x + i\sqrt{3}ak_y} & 0 \end{pmatrix} \tag{5.1}$$

Consider a few values around $r = 1$, which corresponds to no strain, to see how the band structures evolve with increasing r.

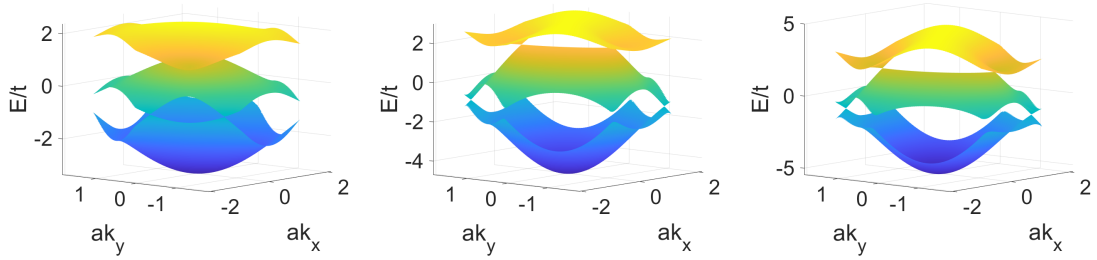

(a) r=0.5 (b) r=1.5 (c) r=2

Figure 15: Energy dispersion of Kagome lattice with strains; when strains are applied, the flat band is no longer present.

Figure (15) shows that at $r = 1.5$, the degeneracies at the K/K' and Γ are lifted but instead the degeneracy at the Γ point is split and pushed outwardly from the centre. Moreover, the top band is no longer flat as soon as r is made differ from 1. This shows that flatness is not protected when these strains are applied and also that the degeneracy is moved to different points.

5.2 Different On-Site Energies in Kagome Lattice

Another modification of Hamiltonian that can be tested is introducing different on-site energies for the three types of atoms. This is always the case when the three atoms in the lattice are of different kinds. This can be reflected in the Hamiltonian by simply adding diagonal elements, which precisely represent the on-site energies of the three atoms. By letting the two atoms, which are represented as the first and third element of the Hamiltonian, have different on-site energies ϵ_1 and ϵ_2, the Hamiltonian can be written in the following manner.

$$H = -t \begin{pmatrix} \epsilon_1 & 1 + e^{-i2ak_x} & 1 + e^{-iak_x - i\sqrt{3}ak_y} \\ 1 + e^{i2ak_x} & 0 & 1 + e^{iak_x - i\sqrt{3}ak_y} \\ 1 + e^{iak_x + i\sqrt{3}ak_y} & 1 + e^{-iak_x + i\sqrt{3}ak_y} & \epsilon_2 \end{pmatrix} \tag{5.2}$$

To examine what happens to the flat band, two scenarios will be considered first; $\epsilon_1 = \epsilon_2$ and $\epsilon_1 = -\epsilon_2$.

5.2.1 $\epsilon_1 = \epsilon_2$

Observe the band structure while paying particular attention to the top flat band as $\epsilon = \epsilon_1 = \epsilon_2$ take a few different values.

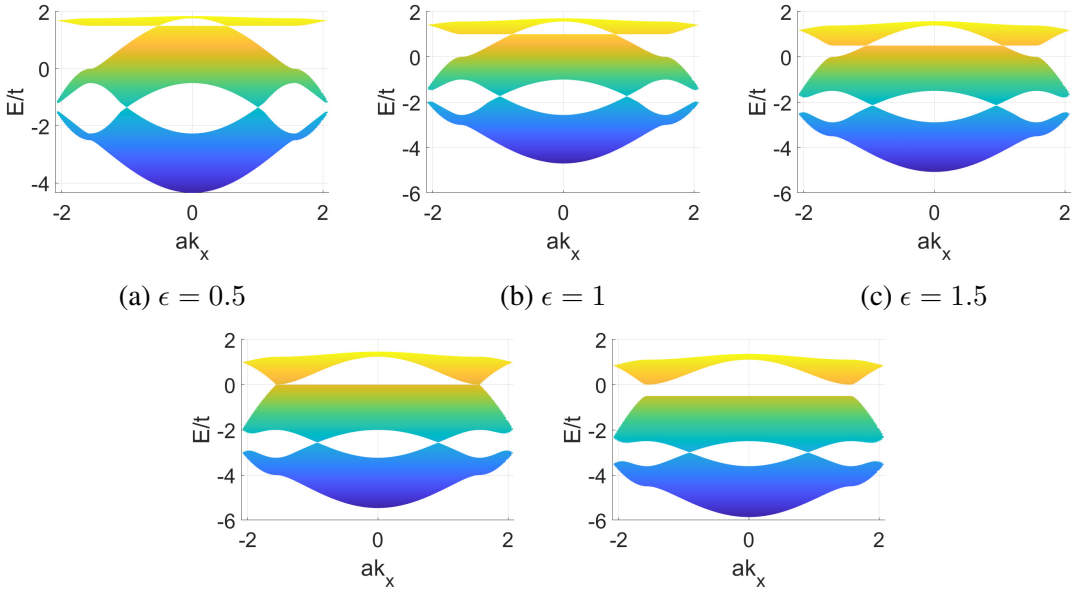

(a) $\epsilon = 0.5$ (b) $\epsilon = 1$ (c) $\epsilon = 1.5$

(d) $\epsilon = 2$ (e) $\epsilon = 2.5$

Figure 16: Variation of band structure of Kagome lattice when the on-site energies of two atoms are equal; flat band is not present again.

As it can be seen in Figure 16, the K/K' and Γ points are not degenerate anymore. At the same time, the top flat band becomes dispersive.

5.2.2 $\epsilon_1 = -\epsilon_2$

Now, examine what happens when the two on-site energies are made negative to each other.

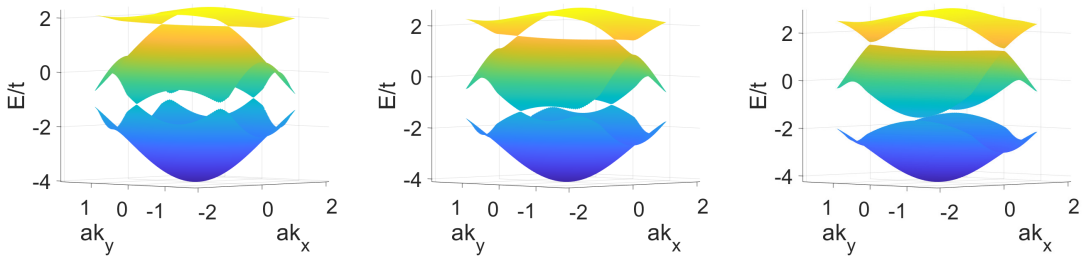

(a) $\epsilon_1 = 0.5$ (b) $\epsilon_1 = 1$ (c) $\epsilon_1 = 1.5$

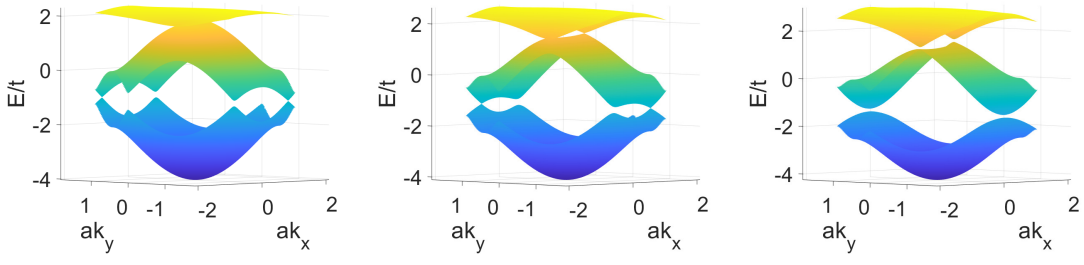

(d) $\epsilon_1 = -0.5$ (e) $\epsilon_1 = -1$ (f) $\epsilon_1 = -1.5$

Figure 17: Band structure of Kagome lattice where two on-site energies are set negative to each other; flat band is no longer present again.

Observe in Figure (17) that the degeneracies at the K/K' and Γ are lifted but the flatness of the top band is no longer preserved.

5.2.3 $\epsilon_2 = r\epsilon_1$

Lastly, let ϵ_1 and ϵ_2 be completely different. Let $\epsilon_2 = r\epsilon_1$ for r any real number. For the purpose of demonstration, r will take two values 2 and 3.

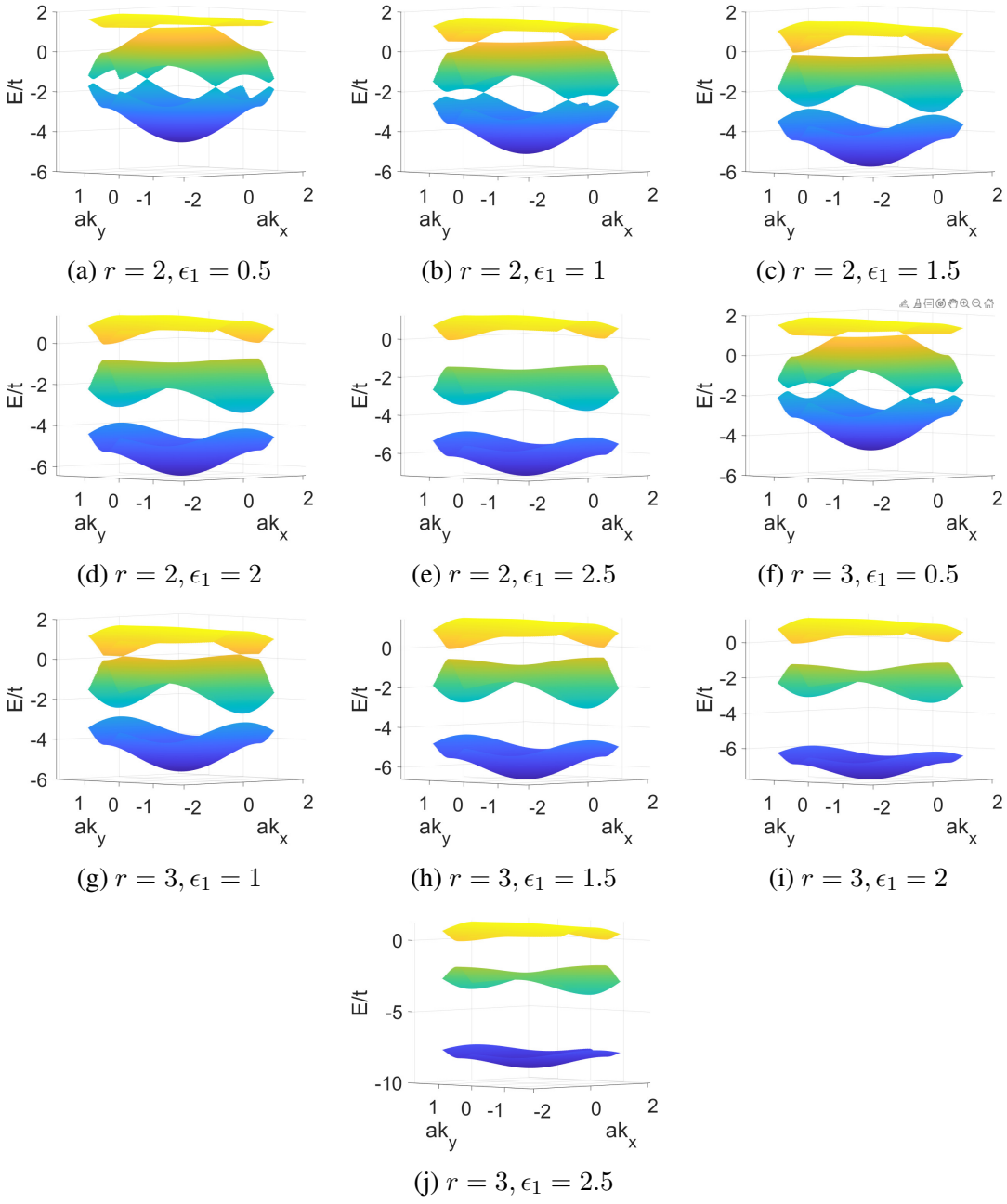

(a) $r = 2, \epsilon_1 = 0.5$ (b) $r = 2, \epsilon_1 = 1$ (c) $r = 2, \epsilon_1 = 1.5$

(d) $r = 2, \epsilon_1 = 2$ (e) $r = 2, \epsilon_1 = 2.5$ (f) $r = 3, \epsilon_1 = 0.5$

(g) $r = 3, \epsilon_1 = 1$ (h) $r = 3, \epsilon_1 = 1.5$ (i) $r = 3, \epsilon_1 = 2$

(j) $r = 3, \epsilon_1 = 2.5$

Figure 18: Band structure of Kagome lattice whose on-site energies are $\epsilon_2 = r\epsilon_1$; whenever the three atoms of Kagome lattice are made different from one another the flat band is absent.

Clearly, adding different on-site energies to the Hamiltonian destroys the flatness in Kagome lattice. This implies that the three types of atoms must be of the same kind. Otherwise, there the system cannot hold a flat band. For the last type of modification of the Hamiltonian in the upcoming sections, it will be assumed that the three atoms are of the same kind and thus have the same on-site energies.

5.3 Modifying Unit Cell in Kagome Lattice

The last modification to the Hamiltonian we consider requires varying the hopping amplitudes by differentiating those of intra-unit cell from those of inter-unit cell.
To distinguish the two types of hopping amplitudes, define the following variables.

$$t_{intra} \equiv t(1+r), \quad t_{inter} \equiv t(1-r) \tag{5.3}$$

r is defined such that increasing r increases t_{intra} while decreasing t_{inter} and vice versa.

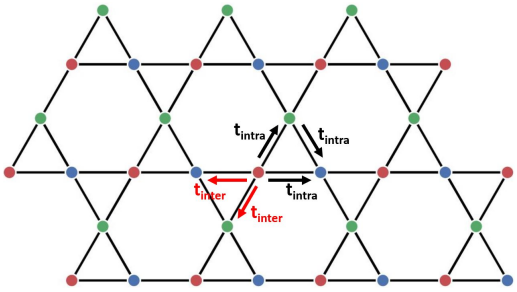

Figure 19: Kagome lattice with varying t_{inter} and t_{intra}

In this way, increasing r weakens t_{inter} and consequently this corresponds to increasing the distance between the unit cells as depicted in Figure (20).

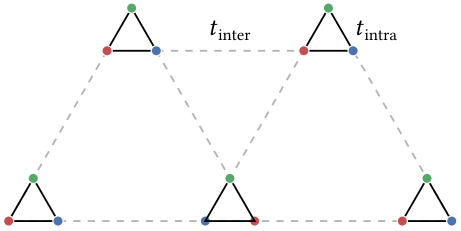

Figure 20: t_{inter} vs t_{intra}; increasing r results in increasing distance between unit cells.

5.3.1 Varying Hopping Amplitudes for $0 \leq r < 1$

First, consider the case where $0 \leq r < 1$, in other words, $t_{intra} \geq t_{inter}$. Here, the effective inter-hopping range is longer and intra-hopping range is shorter. In other words, the distance between unit cells is longer. In this case, the system has stronger intra-molecular bonds than inter-molecular bonds.

The Hamiltonian then can be written as

$$H = -t \begin{pmatrix} 0 & (1+r)+(1-r)e^{ikR_1} & (1+r)+(1-r)e^{ikR_2} \\ (1+r)+(1-r)e^{-ikR_1} & 0 & (1+r)+(1-r)e^{ikR_3} \\ (1+r)+(1-r)e^{-ikR_2} & (1+r)+(1-r)e^{-ikR_3} & 0 \end{pmatrix} \tag{5.4}$$

With the same gauge transformation as the original Kagome lattice, (2.5), the Hamiltonian can be expressed as

$$H = -2t(1+r)e^{\frac{\alpha}{2}} \begin{pmatrix} 0 & \cosh\left(\frac{\alpha+ikR_1}{2}\right) & \cosh\left(\frac{\alpha+ikR_2}{2}\right) \\ \cosh\left(\frac{\alpha-ikR_1}{2}\right) & 0 & \cosh\left(\frac{\alpha+ikR_3}{2}\right) \\ \cosh\left(\frac{\alpha-ikR_2}{2}\right) & \cosh\left(\frac{\alpha-ikR_3}{2}\right) & 0 \end{pmatrix} \tag{5.5}$$

where $\frac{1-r}{1+r} = e^{\alpha}$.

Notice that the form of the Hamiltonian is identical to the form of the original Hamiltonian of Kagome, which is (2.2). Thus, we can follow the precisely the same prescription. If there is a flat band, its associated eigenvalue must satisfy the characteristic polynomial in (2.4). Define $f \equiv \frac{\lambda_c}{2t(1+r)e^{\frac{\alpha}{2}}}$. Thus, the characteristic polynomial writes

$$\begin{aligned} &\left|\cos\left(\frac{kR_1}{2} - i\frac{\alpha}{2}\right)\right|^2 + \left|\cos\left(\frac{kR_2}{2} - i\frac{\alpha}{2}\right)\right|^2 + \left|\cos\left(\frac{kR_3}{2} - i\frac{\alpha}{2}\right)\right|^2 \\ &= \frac{2}{f} Re\left[\cos\left(\frac{kR_1}{2} + i\frac{\alpha}{2}\right)\cos\left(\frac{kR_2}{2} - i\frac{\alpha}{2}\right)\cos\left(\frac{kR_3}{2} + i\frac{\alpha}{2}\right)\right] + f^2 \end{aligned} \tag{5.6}$$

To simplify the equation above, use the following identities (proof found in the Appendix).

$$\sum_{n=1}^{3}\left|\cos\left(\frac{kR_n}{2} - i\frac{\alpha}{2}\right)\right|^2 = \sum_{n=1}^{3}\cos^2\left(\frac{kR_n}{2}\right) + 3\sinh^2\left(\frac{\alpha}{2}\right) \tag{5.7}$$

$$2Re\left[\prod_{n=1}^{3}\cos\left(\frac{kR_n}{2}(-1)^{n+1}i\frac{\alpha}{2}\right)\right] = 2\cosh\left(\frac{\alpha}{2}\right)\prod_{n=1}^{3}\cos\left(\frac{kR_n}{2}\right) + 2\cosh\left(\frac{\alpha}{2}\right)\sinh^2\left(\frac{\alpha}{2}\right) \tag{5.8}$$

$$\sum_{n=1}^{3}\cos^2\left(\frac{kR_n}{2}\right) = 2\prod_{n=1}^{3}\cos\left(\frac{kR_n}{2}\right) + 1 \tag{5.9}$$

Then, equation (5.6) reads

$$2\prod_{n=1}^{3}\cos\left(\frac{kR_n}{2}\right)+1+3\sinh^2\left(\frac{\alpha}{2}\right) \tag{5.10}$$

$$=\frac{2}{f}\left[\cosh\left(\frac{\alpha}{2}\right)\prod_{n=1}^{3}\cos\left(\frac{kR_n}{2}\right)+\cosh\left(\frac{\alpha}{2}\right)\sinh^2\left(\frac{\alpha}{2}\right)\right]+f^2 \tag{5.11}$$

This equation is solved for a constant value (independent of k) $f=\cosh\left(\frac{\alpha}{2}\right)$. Thus, the flat band has energy

$$\lambda=2t(1+r)e^{\frac{\alpha}{2}}\cosh\left(\frac{\alpha}{2}\right)=2t \tag{5.12}$$

The other two remaining eigenvalues can also be computed using equation (4.2).

$$\frac{\lambda_{\pm}}{t}=-1\pm(1+r)e^{\frac{\alpha}{2}}\sqrt{8\prod_{n=1}^{3}\cos\left(\frac{kR_n}{2}\right)+9\sinh^2\left(\frac{\alpha}{2}\right)+1} \tag{5.13}$$

Note that the energy of the flat band is identical to the case $\alpha=0$ (equivalently $r=0$, no modification in Hamiltonian). Furthermore, the eigenvalue of the flat band, f, is independent of r. This implies that the existence of the flat band is not affected when r varies. Furthermore, note that substituting $r=0$ in (5.13) restores the two dispersive eigenvalues of the original Kagome lattice. Hence, we see that there is a family of Hamiltonian parametrized by r.

Now, to see whether the flat band is degenerate with neighbouring bands or not, check condition (4.3).

$$3\cosh^2\left(\frac{\alpha}{2}\right)=\sum_{n=1}^{3}\cos^2\left(\frac{kR_n}{2}\right)+3\sinh^2\left(\frac{\alpha}{2}\right) \tag{5.14}$$

$$\prod_{n=1}^{3}\cos\left(\frac{kR_n}{2}\right)=1 \tag{5.15}$$

The result implies that either all three cosine terms must be equal to 1 or two of them be -1 while the remaining one is 1. In other words, when each $\frac{kR_n}{2}$ is some integral multiple of π, the flat band is degenerate. In the FBZ, this condition is yielded at $\vec{k}=(0,0)$. Moreover, the condition for degeneracy is also independent of r. In other words, the degeneracy is preserved with varying r.

The degeneracy can be identified without having to evaluate the eigenvalues based on the

previous discussion. It can be achieved by using equation (4.12) where the α's correspond to the three elements of the upper triangle in matrix (5.4).

$$|(1+r)+(1-r)e^{ikR_1}|^2 = |(1+r)+(1-r)e^{ikR_{2,3}}|^2 \tag{5.16}$$

$$\begin{aligned}\Rightarrow (1+r)^2+(1-r)^2+2(1+r)(1-r)\cos(kR_1)\\ = (1+r)^2+(1-r)^2+2(1+r)(1-r)\cos(kR_{2,3})\end{aligned}$$

$$\Rightarrow \cos(kR_1)-\cos(kR_{2,3})=0 \tag{5.17}$$

The last line is exactly the same as the condition of double degeneracy when $r = 0$ (section 4.2.3), thus gives $\vec{k} = \left(\frac{n\pi}{3}, \frac{n\pi}{\sqrt{3}}\right)$.

Recall that the constraint that equates the mod square of each of the hopping amplitudes to energy squared did not impose any additional restriction to the $\vec{k}$ value when $r = 0$. With $r \neq 0$, however, this will play a significant role as it will soon be demonstrated. Consider the constraint.

$$|H_{12,23,13}|^2 = E^2 \tag{5.18}$$

$$\Rightarrow |(1+r)+(1-r)e^{ikR_n}|^2 = E^2$$

$$\Rightarrow (1+r)^2+(1-r)^2+2(1+r)(1-r)\cos(kR_n) = E^2 \tag{5.19}$$

If the left-hand side is to be real, either $\cos(kR_n) = \pm 1$ or $r = 0$. $r = 0$ is again the original Hamiltonian in section 4.2.3 and thus the vertices of FBZ manifest double degeneracy. On the other hand, $\cos(kR_n) = \pm 1$ implies that only at $\vec{k} = (0, 0)$ and $\frac{E}{t} = 2$ there is degeneracy, which is independent of r. Thus, it is expected that the six degenerate points at $\frac{E}{t} = -1$ disappear as soon as $r \neq 0$ whereas the degeneracy between the top flat band and the middle band is preserved regardless of change in r. This means that varying r only influences the dispersion of the two dispersive bands. The top flat band in Figure (2) remains unchanged and the middle dispersive band goes through deformation with varying r. This can also be visually verified in Figure (21).

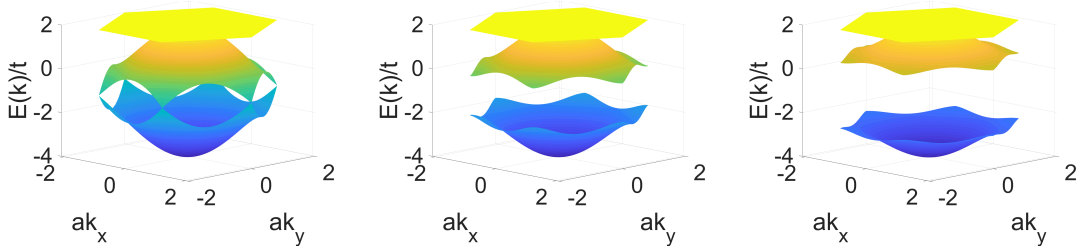

(a) $r = 0$ (b) $r = 0.3$ (c) $r = 0.5$

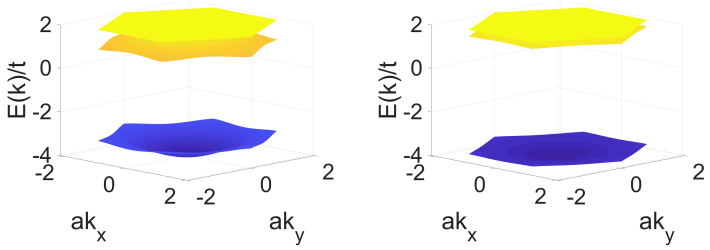

(d) $r = 0.7$ (e) $r = 0.9$

Figure 21: Band structures of Kagome lattice for $t_{intra} \geq t_{inter}$ ($r \in [0, 1[$); both flat band and degeneracy are preserved.

5.3.2 Hopping Amplitudes for $r > 1$

In order to complete the analysis of the effect of varying r, also consider the case $r > 1$. Notice that this case implies $t_{inter} = (1-r) < 0$ This does not have a physical meaning in solid crystals but it is realizable in optical lattices, where the coupling between atomic sites can carry a phase. The corresponding Hamiltonian reads

$$H = -t \begin{pmatrix} 0 & (1+r)+(1-r)e^{ikR_1} & (1+r)+(1-r)e^{ikR_2} \\ (1+r)+(1-r)e^{-ikR_1} & 0 & (1+r)+(1-r)e^{ikR_3} \\ (1+r)+(1-r)e^{-ikR_2} & (1+r)+(1-r)e^{-ikR_3} & 0 \end{pmatrix} \tag{5.20}$$

Factor out $(1+r)$ like before. But this time, $\frac{1-r}{1+r} \neq e^{\alpha}$ because the left hand side of the equation is negative. Then, define $\frac{1-r}{1+r} = e^{\alpha+i\pi}$ such that $e^{\alpha} = \left|\frac{1-r}{1+r}\right|$.

With the gauge transformation (2.5) Hamiltonian can be expressed as

$$H = -2t(1+r)e^{\frac{\alpha}{2}} \begin{pmatrix} 0 & i\cosh\left(\frac{\alpha+i\pi+ikR_1}{2}\right) & i\cosh\left(\frac{\alpha+i\pi+ikR_2}{2}\right) \\ -i\cosh\left(\frac{\alpha-i\pi-ikR_1}{2}\right) & 0 & i\cosh\left(\frac{\alpha+i\pi+ikR_3}{2}\right) \\ -i\cosh\left(\frac{\alpha-i\pi-ikR_2}{2}\right) & i\cosh\left(\frac{\alpha-i\pi-ikR_3}{2}\right) & 0 \end{pmatrix} \tag{5.21}$$

The above Hamiltonian takes the form of the original Kagome lattice again, (2.2). Then, following the same scheme, the characteristic equation of the Hamiltonian is

$$\lambda^3 - \lambda\left(|\alpha_1|^2 + |\alpha_2|^2 + |\alpha_3|^2\right) + 2Re\left[\alpha_1^*\alpha_2\alpha_3^*\right] = 0 \tag{5.22}$$

By defining $f = \frac{\lambda}{2t(1+r)e^{\frac{\alpha}{2}}}$ for the flat band, the charactersitic polynomial can be written as

$$f\sum_{n=1}^{3}\left|sin\left(\frac{kR_n - i\alpha}{2}\right)\right|^2 = -2Im\prod_{n=1}^{3} sin\left(\frac{kR_n - \alpha(-1)^n}{2}\right) + f^3 \tag{5.23}$$

To simplify the equation above, consider the following identities (for $r > 1$, proof found in the Appendix).

$$\sum_{n=1}^{3}\left|sin\left(\frac{kR_n - \alpha}{2}\right)\right|^2 = -1 - 2\prod_{n=1}^{3}\cos\left(\frac{kR_n}{2}\right) + 3\cosh^2\left(\frac{\alpha}{2}\right) \tag{5.24}$$

$$2Im\prod_{n=1}^{3} sin\left(\frac{kR_n - \alpha(-1)^n}{2}\right) = -2\sinh\left(\frac{\alpha}{2}\right)\prod_{n=1}^{3}\cos\left(\frac{kR_n}{2}\right) + 2\sinh\left(\frac{\alpha}{2}\right)\cosh^2\left(\frac{\alpha}{2}\right) \tag{5.25}$$

Then, the characteristic polynomial can be rewritten as

$$\begin{aligned} &f\left[-1 - 2\prod_{n=1}^{3}\cos\left(\frac{kR_n}{2}\right) + 3\cosh^2\left(\frac{\alpha}{2}\right)\right] \\ &= 2\sinh\left(\frac{\alpha}{2}\right)\prod_{n=1}^{3}\cos\left(\frac{kR_n}{2}\right) - 2\sinh\left(\frac{\alpha}{2}\right)\cosh^2\left(\frac{\alpha}{2}\right) + f^3 \end{aligned} \tag{5.26}$$

This equation is solvable with $f = -\sinh\left(\frac{\alpha}{2}\right)$, again independent of k. One can immediately see that the flat band has energy

$$\lambda = 2t(1+r)e^{\frac{\alpha}{2}}\left[-\sinh\left(\frac{\alpha}{2}\right)\right] = 2t \tag{5.27}$$

Using equation (4.2), the other two eigenvalues can also be found.

$$\frac{\lambda_{\pm}}{2t(1+r)e^{\frac{\alpha}{2}}} = \frac{-\sinh\left(\frac{\alpha}{2}\right)\sqrt{4\left[-1-2\prod_{n=1}^{3}\cos\left(\frac{kR_n}{2}\right)+3\cosh^2\left(\frac{\alpha}{2}\right)\right]-3\sinh^2\left(\frac{\alpha}{2}\right)}}{2} \tag{5.28}$$

$$\Rightarrow \lambda_{\pm} = t\left(-1\mp(1+r)e^{\frac{\alpha}{2}}\sqrt{-8\prod_{n=1}^{3}\cos\left(\frac{kR_n}{2}\right)+9\cosh^2\left(\frac{\alpha}{2}\right)-1}\right) \tag{5.29}$$

Then for the degeneracy, consider equation (4.3) again.

$$3\sinh^2\left(\frac{\alpha}{2}\right) = -1-2\prod_{n=1}^{3}\cos\left(\frac{kR_n}{2}\right)+3\cosh^2\left(\frac{\alpha}{2}\right) \tag{5.30}$$

$$\Rightarrow \prod_{n=1}^{3}\cos\left(\frac{kR_n}{2}\right) = 1 \tag{5.31}$$

The same conclusion is drawn as in the case $0 \leq r < 1$. Note also that based on the method discussed in the previous chapter, imposing condition (4.12) to the Hamiltonian gives exactly the same result as the case $0 \leq r < 1$. The degeneracy between the top flat band and the middle dispersive band is preserved throughout the change in r. The degeneracy between the middle and the bottom bands disappears as soon as $r \neq 0$. The inferences agree with the band structures obtained by brute-force diagonalizing the Hamiltonian in Figure (22).

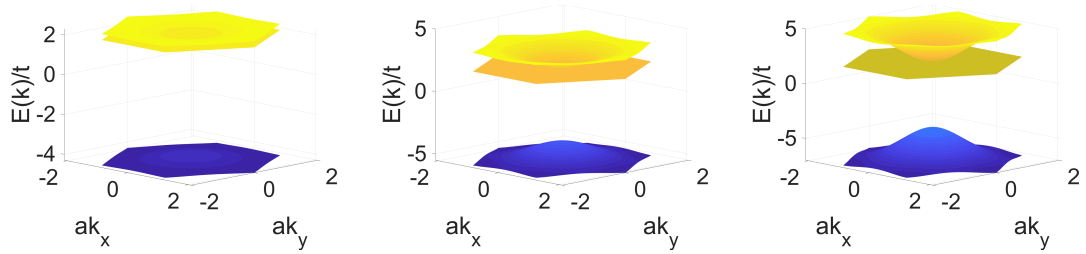

(a) $r = 1.1$ (b) $r = 1.5$ (c) $r = 2$

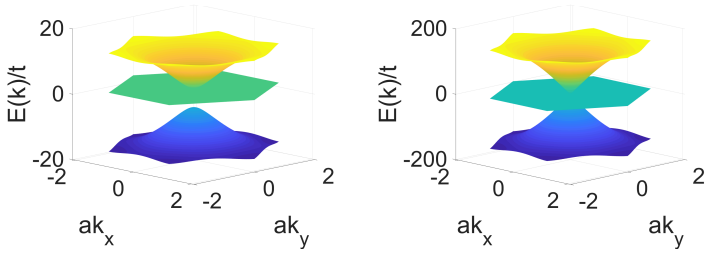

(d) $r = 5$ (e) $r = 50$

Figure 22: Band structure of Kagome lattice for $t_{intra} < t_{inter}$ $(r > 1)$; flat band and degeneracy are protected.

5.3.3 Case $r = 1$

Consider Figure (21, e) and Figure (22, a) . When r is close to 1 ($t_{inter} \approx 0$), the two dispersive bands seem to flatten out. In particular, the middle band overlaps with the top band as it becomes flatter. This can be shown mathematically as well. Consider taking a limit of the eigenvalues of the case $0 \leq r < 1$ first.

$$\lim_{r\to 1^-} \lambda_{\pm} = \lim_{r\to 1^-} t \left(-1 \pm (1+r)e^{\frac{\alpha}{2}} \sqrt{8 \prod_{n=1}^{3} \cos(\frac{kR_n}{2}) + 9\sinh^2(\frac{\alpha}{2}) + 1} \right) \tag{5.32}$$

Here,

$$\lim_{r\to 1^-} e^{\frac{\alpha}{2}}\sqrt{8\prod_{n=1}^{3}\cos(\frac{kR_n}{2})+9\sinh^2(\frac{\alpha}{2})+1} \tag{5.33}$$

$$= \lim_{r\to 1^-}\sqrt{e^{\alpha}8\prod_{n1}^{3}\cos(\frac{kR_n}{2})+e^{\alpha}9\sinh^2(\frac{\alpha}{2})+e^{\alpha}} \tag{5.34}$$

$$= \lim_{r\to 1^-}\sqrt{\frac{9}{4}e^{\alpha}\left(e^{\frac{\alpha}{2}}-e^{-\frac{\alpha}{2}}\right)^2} \tag{5.35}$$

$$= \lim_{r\to 1^-}\frac{3}{2}\sqrt{e^{2\alpha}-2e^{\alpha}+1} \tag{5.36}$$

$$= \lim_{r\to 1^-}\frac{3}{2}\sqrt{\left(\frac{1-r}{1+r}\right)^2-2\left(\frac{1-r}{1+r}\right)+1} \tag{5.37}$$

$$= \frac{3}{2} \tag{5.38}$$

Thus,

$$\lim_{r\to 1^-}\lambda_{\pm} = t\,(-1\pm 3)$$

$$= -4t,\ 2t$$

As mentioned before, the eigenvalue corresponding to the top flat band is independent of r and taking the limit for r still gives the same value $2t$. Thus, all three bands end up being flat with energies -4t, 2t, and 2t. λ_+ overlaps with the top band as it was shown in the figures above. This can also be seen from other the side, $r > 1$. Consider the eigenvalues and take the appropriate limit again.

$$\lim_{r\to 1^+}\lambda_{\pm} = \lim_{r\to 1^+} t\left(-1\mp(1+r)e^{\frac{\alpha}{2}}\sqrt{-8\prod_{n=1}^{3}\cos(\frac{kR_n}{2})+9\cosh^2(\frac{\alpha}{2})-1}\right) \tag{5.39}$$

Here,

$$\lim_{r\to 1^+} e^{\frac{\alpha}{2}} \sqrt{-8\prod_{n=1}^{3}\cos(\frac{kR_n}{2}) + 9\cosh^2(\frac{\alpha}{2}) - 1} \tag{5.40}$$

$$= \lim_{r\to 1^+} \sqrt{-e^{\alpha}8\prod_{n=1}^{3}\cos(\frac{kR_n}{2}) + e^{\alpha}9\cosh^2(\frac{\alpha}{2}) - e^{\alpha}} \tag{5.41}$$

$$= \lim_{r\to 1^+} \frac{3}{2}\sqrt{e^{\alpha}\left(e^{\frac{\alpha}{2}} + e^{-\frac{\alpha}{2}}\right)^2} \tag{5.42}$$

$$= \frac{3}{2}\lim_{r\to 1^+} \sqrt{e^{2\alpha} + 2e^{\alpha} + 1} \tag{5.43}$$

$$= \frac{3}{2}\lim_{r\to 1^+} \sqrt{\left(\frac{r-1}{r+1}\right)^2 + 2\left(\frac{r-1}{r+1}\right) + 1} \tag{5.44}$$

$$= \frac{3}{2} \tag{5.45}$$

Thus,

$$\lim_{r\to 1^+} \lambda_{\pm} = t\left(-1 \mp 3\right)$$
$$= -4t,\, 2t$$

Again, the top flat band corresponds to the eigenvalue $2t$, which is independent of k. As presumed, exactly the same results are drawn in both sides. As r approaches 1, all three bands flatten out. This is because $r = 1$ means $t_{inter} = 0$, which implies that the unit cells are completely isolated from one another. In other words, electrons are trapped by the atoms and no matter how much momentum the electrons possess, they will be in one of the three orbitals in the atom. Atomic orbitals, when isolated from a lattice structure, have non-dispersive energy structure. The energies of these orbitals are precisely where the flat bands are sitting.

5.3.4 Case $r < 0$

Let r be less than zero. This implies that $t_{intra} \leq t_{inter}$. As mentioned previously, decreasing r implies decreasing the distance between unit cells. $r = 0$ is the point where the inter-unit-cell distance is same as intra-unit-cell distance (no distinction between t_{intra} and t_{inter}). When $r > 0$, the inter-unit-cell distance is larger than the intra-unit-cell distance and vice versa. It can be easily seen that the case $-1 < r < 0$ follows the same calculations and have the same results as the case $0 < r < 1$. Similarly, the case $r < -1$ is identical to the case $r > 1$. Figures (21) and (22) portray the same evolution of the band structure as Figures (23) and (24).

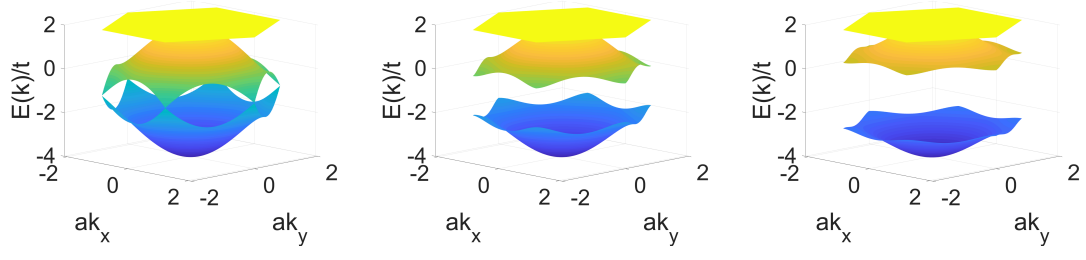

(a) $r = -0.1$ (b) $r = -0.3$ (c) $r = -0.5$

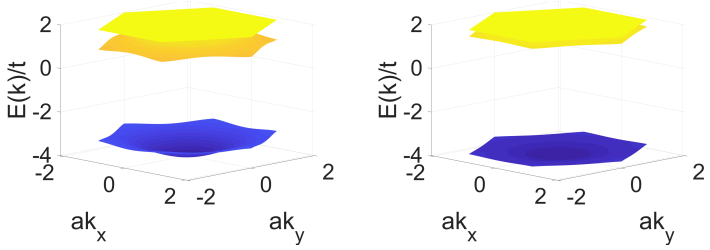

(d) $r = -0.7$ (e) $r = -0.9$

Figure 23: Band structures of Kagome lattice for $-1 < r < 0$; the band structure evolves in the same manner as $0 < r < 1$.

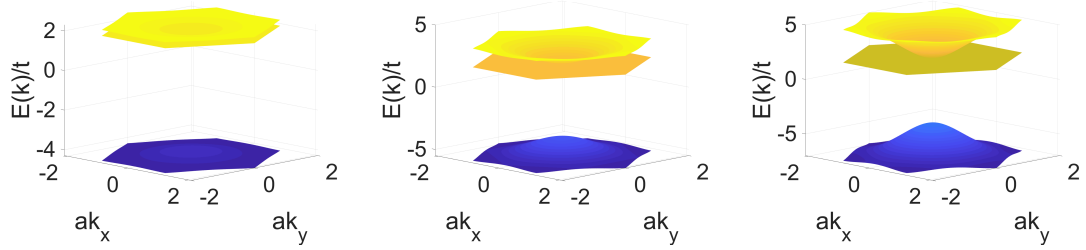

(a) $r = -1.1$ (b) $r = -1.5$ (c) $r = -2$

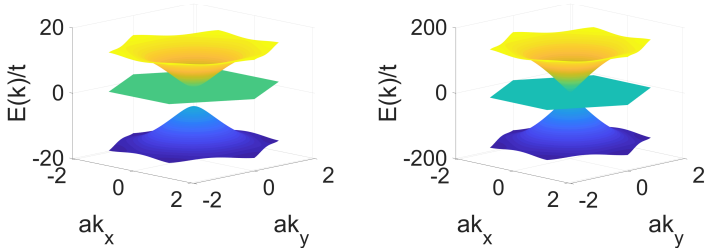

(d) $r = -5$ (e) $r = -50$

Figure 24: Band structures of Kagome lattice for $r < -1$; the band structure evolves again in the same manner as the case $r > 1$.

In conclusion, increasing t_{intra} at the cost of decreasing t_{inter} in the positive r regime has the same effect on the lattice as increasing t_{inter} and decreasing t_{intra} in the negative r regime.

Refer to Figure (25). Increasing t_{inter} in (a) is equivalent to increasing t_{intra} in (b). Taking into account the fact that both represent the same Kagome lattice, it can be seen that the two actions have the identical effect on the lattice in terms of energy. Nevertheless, the wavefunction can carry information about the topology. It is left for a future investigation to study the topological distinction between the two cases.

(a) $r > 0$ (b) $r < 0$

Figure 25: Increasing t_{intra} in $r > 0$ and increasing t_{inter} in $r < 0$ have the same effect on the energy.

5.4 Modifying the Unit Cell in the Lieb Lattice

Just like the case of Kagome lattice, define r in order to differentiate the inter-unit-cell hopping amplitudes from the intra-unit-cell hopping amplitudes.

$$t_{intra} \equiv t(1+r), \quad t_{inter} \equiv t(1-r) \tag{5.46}$$

Again, increase in r implies increase in t_{intra} and decrease in t_{inter} at the same time as well as increase in distance between unit cells.

5.4.1 Varying Hopping Amplitudes for $0 \leq r < 1$

Consider the case $0 \leq r < 1$, or $t_{intra} \geq t_{inter}$. The Hamiltonian can be expressed as

$$H = -t \begin{pmatrix} 0 & (1+r)+(1-r)e^{ikR_1} & (1+r)+(1-r)e^{ikR_2} \\ (1+r)+(1-r)e^{-ikR_1} & 0 & 0 \\ (1+r)+(1-r)e^{-ikR_2} & 0 & 0 \end{pmatrix} \tag{5.47}$$

Define $e^{\alpha} = \frac{1-r}{1+r}$ such that with the gauge transformation (2.5) the Hamiltonian is written as

$$-2t(1+r)e^{\frac{\alpha}{2}} \begin{pmatrix} 0 & \cosh\left(\frac{\alpha+ikR_1}{2}\right) & \cosh\left(\frac{\alpha+ikR_2}{2}\right) \\ \cosh\left(\frac{\alpha-ikR_1}{2}\right) & 0 & 0 \\ \cosh\left(\frac{\alpha-ikR_2}{2}\right) & 0 & 0 \end{pmatrix} \tag{5.48}$$

The flat band is still held at $\lambda = 0$ and the other two eigenvalues can be computed also.

$$\frac{\lambda_{\pm}}{t(1+r)e^{\frac{\alpha}{2}}} = \pm\sqrt{\left|2\cosh\left(\frac{\alpha+ikR_1}{2}\right)\right|^2 + \left|2\cosh\left(\frac{\alpha+ikR_2}{2}\right)\right|^2} \tag{5.49}$$

$$\Rightarrow \lambda_{\pm} = \pm t(1+r)e^{\frac{\alpha}{2}}\sqrt{4\cosh(\alpha) + 2\cos(kR_1) + 2\cosh(kR_2)} \tag{5.50}$$

The system yields degeneracy at the points that satisfy the following condition.

$$0 = \left|2\cosh\left(\frac{\alpha+ikR_1}{2}\right)\right|^2 + \left|2\cosh\left(\frac{\alpha+ikR_2}{2}\right)\right|^2 \tag{5.51}$$

$$\Rightarrow -2\cosh(\alpha) = \cos(kR_1) + \cos(kR_2) \tag{5.52}$$

Notice that for $0 < r < 1$, $-2\cosh(\alpha) < -2$ and thus the equality above cannot hold. Only when $r = 0$, the two sides can be made equal. While the flat band is present independent of r, the degeneracy is lifted as soon as $r \neq 0$. In other words, the flat band is successfully isolated from the neighbouring bands as soon as the intra-unit-cell and inter-unit-cell hopping amplitudes are differentiated. Observe in Figure (26), obtained by diagonalizing the Hamiltonian at various r, that the degeneracy fades away as soon as r differs from zero while the flat band in the middle remains unchanged.

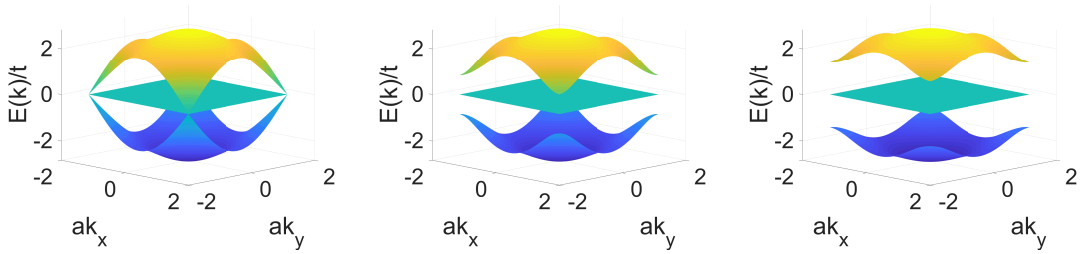

(a) $r = 0$ (b) $r = 0.3$ (c) $r = 0.5$

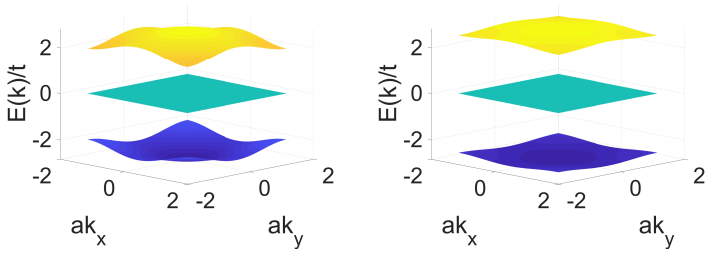

(d) $r = 0.7$ (e) $r = 0.9$

Figure 26: Band structures of Lieb lattice for $0 \leq r < 1$; flat band is protected when r is varied while degeneracy is lifted as soon as r differs from 0.

5.4.2 Hopping Amplitudes for $r > 1$

Let $r > 1$ and define $e^{\alpha} = \frac{1-r}{1+r}$. The Hamiltonian is now

$$H = -2t(1+r)e^{\frac{\alpha}{2}} \begin{pmatrix} 0 & i\cosh\left(\frac{\alpha+i\pi+ikR_1}{2}\right) & i\cosh\left(\frac{\alpha+i\pi+ikR_2}{2}\right) \\ -i\cosh\left(\frac{\alpha-i\pi-ikR_1}{2}\right) & 0 & 0 \\ -i\cosh\left(\frac{\alpha-i\pi-ikR_2}{2}\right) & 0 & 0 \end{pmatrix} \tag{5.53}$$

It can be easily deduced that the flat band is at $\lambda = 0$. The other two eigenvalues are

$$\lambda_{\pm} = \pm t(1+r)e^{\frac{\alpha}{2}}\sqrt{4\cosh(\alpha) - 2\cos(kR_1) - 2\cos(kR_2)} \tag{5.54}$$

For degeneracy to be present, the following equality must hold.

$$0 = \left|i\cosh\left(\frac{\alpha+i\pi+ikR_1}{2}\right)\right|^2 + \left|i\cosh\left(\frac{\alpha+i\pi+ikR_2}{2}\right)\right|^2 \tag{5.55}$$

$$\Rightarrow -2\cosh(\alpha) = \cos(\pi+kR_1) + \cos(\pi+kR_2) \tag{5.56}$$

In the limit where r approaches infinity, the two sides of the equality can be made equal at -2. This is achieved at $\vec{k} = (0,0)$. Figure (27) is obtained by diagonalizing the Hamiltonian at

various values of r. It can be observed that as r increases the two dispersive bands approach the flat band at the origin.

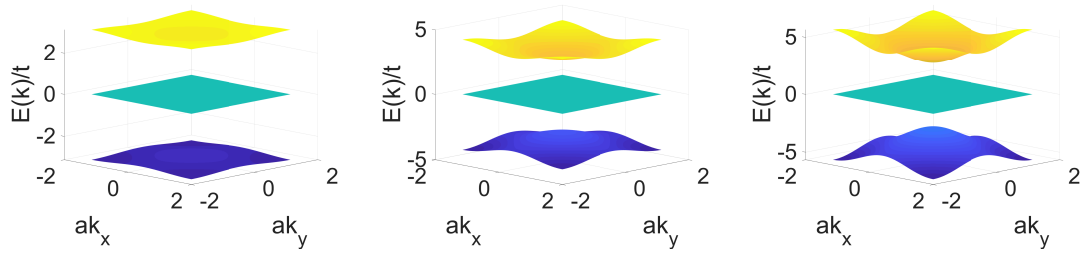

(a) $r = 1.1$ (b) $r = 1.5$ (c) $r = 2$

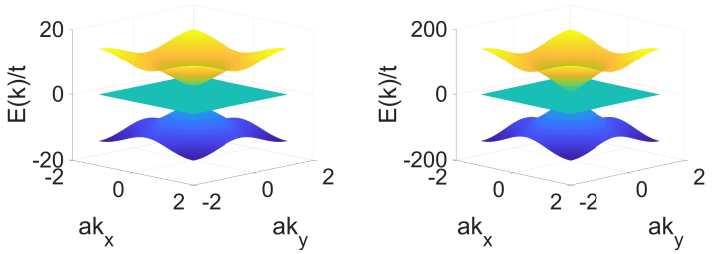

(d) $r = 5$ (e) $r = 50$

Figure 27: Band structure of Lieb lattice for $r > 1$; flat band is still preserved and degeneracy remains lifted.

It is concluded that the flat band is preserved for all values of r while the degeneracy is lifted as soon as r becomes finite. But degeneracy is gradually recovered at a different point, $\vec{k} = (0, 0)$, as r approaches infinity. When r approaches infinity, the ratio between t_{inter} and t_{intra} corresponds to -1. This can be identified as the lattice containing a phase of ϕ, which gives a negative sign to the associated hopping amplitude.

5.4.3 Case $r = 1$

To complete the analysis, consider $r = 1$. First of all, take the eigenvalues of case $r > 1$.

$$\lambda_{\pm} = \pm t(1+r)\sqrt{\frac{r-1}{r+1}}\sqrt{4\left(\frac{r^2+1}{r^2-1}\right) - 2\cos(kR_1) - 2\cos(kR_2)} \tag{5.57}$$

$$= \pm t(1+r)(\pm i)\sqrt{\frac{1-r}{1+r}}(\pm i)\sqrt{4\left(\frac{1+r^2}{1-r^2}\right) + 2\cos(kR_1) + 2\cos(kR_2)} \tag{5.58}$$

$$= \pm t(1+r)\sqrt{\frac{1-r}{1+r}}\sqrt{4\left(\frac{1+r^2}{1-r^2}\right) + 2\cos(kR_1) + 2\cos(kR_2)} \tag{5.59}$$

The last line is exactly the same as the solution of case $0 \leq r < 1$. Thus, Regardless of whether r is greater than 1 or less than 1, the eigenvalues can be found using the same expression.
In order to evaluate the eigenvalues at $r = 1$, modify the expression slightly.

$$\lambda_{\pm} = \pm t(1+r)\sqrt{\frac{1-r}{1+r}}\sqrt{4\left(\frac{1+r^2}{1-r^2}\right) + 2\cos(kR_1) + 2\cos(kR_2)} \tag{5.60}$$

$$= \pm t(1+r)\sqrt{4\left(\frac{1-r}{1+r}\right)\left(\frac{1+r^2}{1-r^2}\right) + \left(\frac{1-r}{1+r}\right)[2\cos(kR_1) + 2\cos(kR_2)]} \tag{5.61}$$

$$= \pm t(1+r)\sqrt{4\frac{1+r^2}{(1+r)^2} + \left(\frac{1-r}{1+r}\right)[2\cos(kR_1) + 2\cos(kR_2)]} \tag{5.62}$$

$r = 1$ can be substituted in the last expression.

$$\lambda_{\pm} = \pm 4t\sqrt{\frac{1}{2}} = \pm 2\sqrt{2}t \approx \pm 2.8284t \tag{5.63}$$

In fact, this result agrees with Figure (26, e) and (27, a). The two dispersive bands at the top and bottom asymptotically approach flatness at $\frac{E}{t} \approx \pm 2.8284$.

5.4.4 Case $r < 0$

It can be easily seen that the case $-1 < r < 0$ follows the same calculations and have the same result as the case $0 < r < 1$. Similarly, the case $r < -1$ is identical to the case $r > 1$.

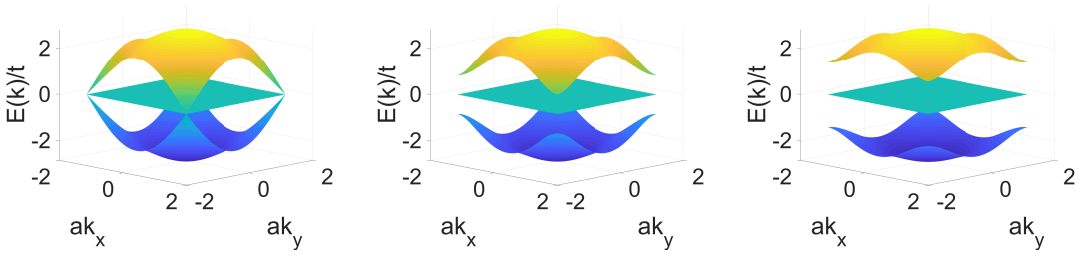

(a) $r = -0.1$ (b) $r = -0.3$ (c) $r = -0.5$

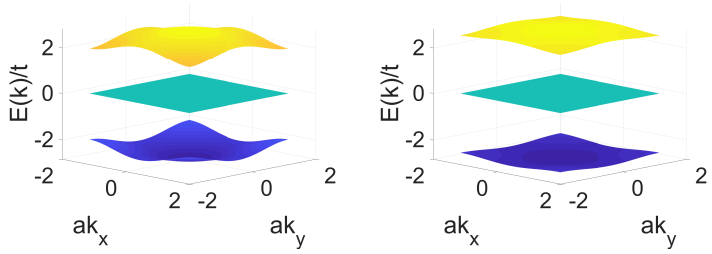

(d) $r = -0.7$ (e) $r = -0.9$

Figure 28: Band structure of Kagome lattice for $-1 < r < 0$; the band structures are reflections of the case $0 < r < 1$.

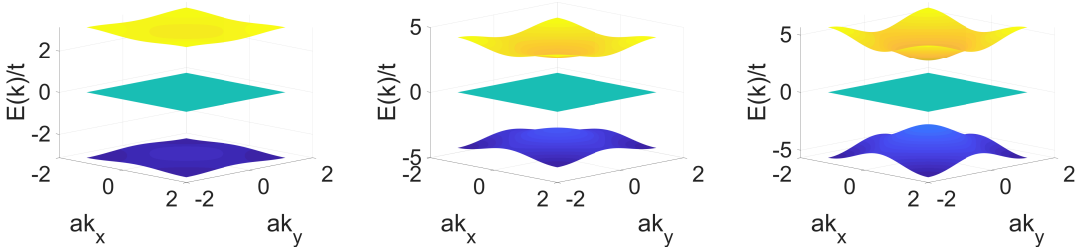

(a) $r = -1.1$ (b) $r = -1.5$ (c) $r = -2$

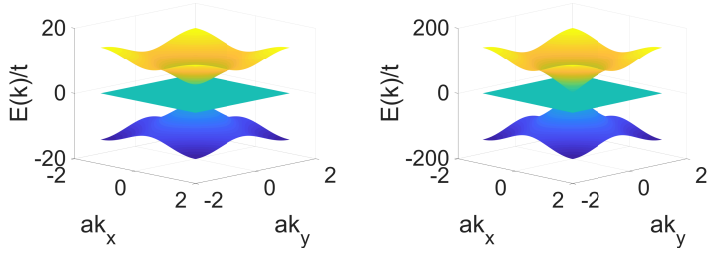

(d) $r = -5$ (e) $r = -50$

Figure 29: Band structure of Kagome lattice for $r < -1$; the band structures evolve in the same way as the case $r > 1$.

Similarly to the case of Kagome lattice, there is no distinction between the cases $r > 0$ and

$r < 0$ as long as the energy is concerned but the wave function may carry information about the topology which may be distinct in the two cases. This can be visually verified in Figure (30).

(a) $r < 0$ (b) $r > 0$

Figure 30: Increasing t_{intra} in $r < 0$ and t_{inter} in $r > 0$ have identical effect on energy.

5.5 Additional Hopping Amplitude in Lieb Lattice

In section 5.4.1, when increasing t_{intra} and decreasing t_{inter}, it was assumed that the same bonds between the nearest neighbours stretched and compressed. At some point, however, the bond between atoms indexed 2 and 3 becomes no longer negligible compared to t_{inter}. Including the contribution from this bond, the Hamiltonian can be written as

$$H = -t \begin{pmatrix} 0 & (1+r)+(1-r)e^{ikR_1} & (1+r)+(1-r)e^{ikR_2} \\ (1+r)+(1-r)e^{-ikR_1} & 0 & s \\ (1+r)+(1-r)e^{-ikR_2} & s & 0 \end{pmatrix} \tag{5.64}$$

where st is the new hopping amplitude. It is worthwhile to study the effect of this new hopping amplitude on the flat band and its degeneracy. First of all, observe in Figure (31) what happens to degeneracy as r and s vary.

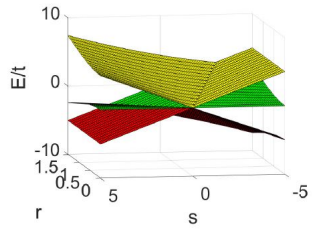

Figure 31: Energies at K point; the triple degeneracy at $(r, s) = (0, 0)$ (no modification in Hamiltonian) is lifted as soon as the Hamiltonian is modified.

At $(r, s) = (0, 0)$, K points are triply degenerate as it is expected. Furthermore, the top two bands remain (doubly) degenerate along a line in rs plane as well as the bottom two bands

(along a different line). This implies that when $(r, s) \neq (0, 0)$, the triple degeneracy at K points is either lifted or transforms into double degeneracy.

5.5.1 Effect of New Hopping Amplitude

In order to see if the flat band remains, the band structure at arbitrary values of r and s can be plotted. Without the loss of generality, r can be fixed at 0.5 while s varies.

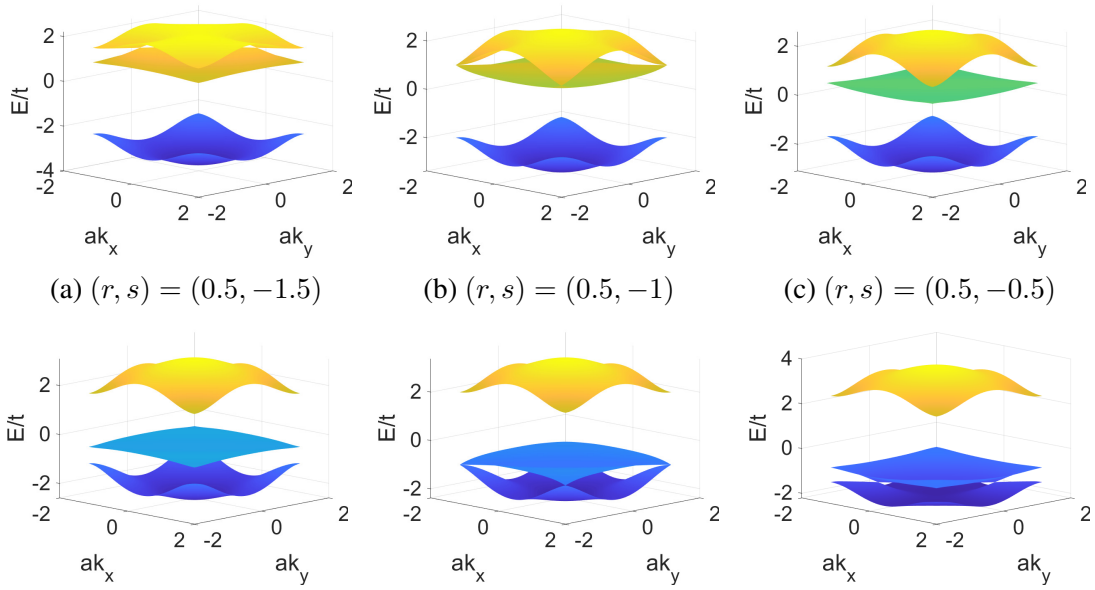

(a) $(r, s) = (0.5, -1.5)$ (b) $(r, s) = (0.5, -1)$ (c) $(r, s) = (0.5, -0.5)$

(d) $(r, s) = (0.5, 0.5)$ (e) $(r, s) = (0.5, 1)$ (f) $(r, s) = (0.5, 1.5)$

Figure 32: Lieb lattice with new hopping amplitude st at $r = 0.5$ and varying s; in all cases the middle band loses its flatness.

It is clear that the Lieb lattice no longer possesses the flat band. In particular, Figure (32, e) and (32, h) correspond to the occurrence of double degeneracy discussed earlier with the two lines in Figure (31). Hence, introducing the new hopping amplitude is not helpful in preserving the flat band. In other words, to keep the flat band while stretching the bonds it has to be manipulated such that the bond between atoms 2 and 3 remains negligible.

5.6 Summary

This chapter explored various modifications of Hamiltonians of Kagome lattice and Lieb lattice. The strains applied to Kagome lattice shifted the degeneracy of the flat band as the ratio between the hopping amplitudes along the edges of the unit cell and those along the internal bonds vary. It was observed that the flatness is immediately lost when this ratio differs from 1. It was also shown that when the three atoms are made different from one another by giving

them different on-site energies, the flat band was no longer present. With the last modification of differentiating t_{inter} from t_{intra}, the flat band was preserved for any ratio between the two types of hopping amplitudes. A similar result was observed with the Lieb lattice. The modification by distinguishing t_{inter} from t_{intra} was shown to preserve the flat band. In both cases, varying the ratio of t_{inter} and t_{intra} produced a family of flat band systems that are practical due to short-range hoppings.

6 Chern-Simons Field

Chern-Simons (CS) theory is limited to 2+1 dimensional (2 spatial and 1 temporal) systems [28]. CS theory,like the Maxwell theory, describes the dynamics of a gauge field. Maxwell theory, however, is not limited to any dimensions. Moreover, one cannot apply a CS field like one can apply a magnetic field. CS field seems to arise out of many-body interactions in flat band systems. The CS-type field emerges if (and only if) time-reversal symmetry or inversion symmetry is broken given that the system has nontrivial topology. Moreover, CS field seems to be relevant in systems with perfectly flat band. Thus, systems with isolated flat bands with broken TRS (or inversion symmetry) and interacting particles are expected to be subjected to CS-like field. Isolating flat bands will allow us to explore this idea.

When the criteria for the CS field are met, the CS field and the Maxwell field can coexist. In this case, the CS field turns out to be more dominant. Furthermore, as a consequence of CS field, magnetic flux is pinned to the charges (electrons). In other words, wherever there is a charge, there is an associated magnetic flux and vice versa. When the charge travels, the flux follows along with it.

The CS gauge field and the corresponding magnetic field can be written as following [28].

$$A^i(\vec{x}_a) = \frac{e}{2\pi\kappa}\sum_{b\neq a}^{N}\epsilon^{ij}\frac{(x_a^j - x_b^j)}{|\vec{x}_a - \vec{x}_b|^2} \tag{6.1}$$

$$B(\vec{x}_a) = \frac{\epsilon}{\kappa}\sum_{b\neq a}^{N}\delta(\vec{x}_a - \vec{x}_b) \tag{6.2}$$

Here, N is the number of particles, $\vec{x}_a$ is the coordinates of the a-th particle, and κ is known as CS coupling parameter. κ is precisely what links the magnetic flux to the charge. When $\frac{1}{\kappa}$ is zero, CS field is absent.

The associated flux can be calculated.

$$\Phi = \int \sum_{b\neq a}^{N}\frac{e}{\kappa}\delta(\vec{x} - \vec{x}_b)\hat{z}\cdot d\vec{s} \tag{6.3}$$

$$= \frac{e}{\kappa}\sum_{b\neq a}^{N}\int\int \delta(x - x_b)\delta(y - y_b)dxdy \tag{6.4}$$

$$= \frac{e}{\kappa}m \tag{6.5}$$

where m corresponds to the number of charges in the area defined by $\int\int dxdy$. In the second line, the integral of delta functions is equal to 1 for each charge indexed with b in the area. What

is implied here is that the flux a charge experiences comes from the mean field approximation of other charges in the given area where each of these charges contributes an amount of $\frac{e}{\kappa}$. As a result, the flux depends on the number of charges in the given area and not the area itself. This is different from the Maxwell field, where the flux is dependent on the covered area.

6.1 CS Field on Kagome Lattice

Returning to the discussion of lattices, the effect of CS field on lattices is redistribution of flux in the unit cell. In the case of Kagome lattice, CS field modulates the flux such that the flux is concentrated in one region of the unit cell as described in Figure (33) [29].

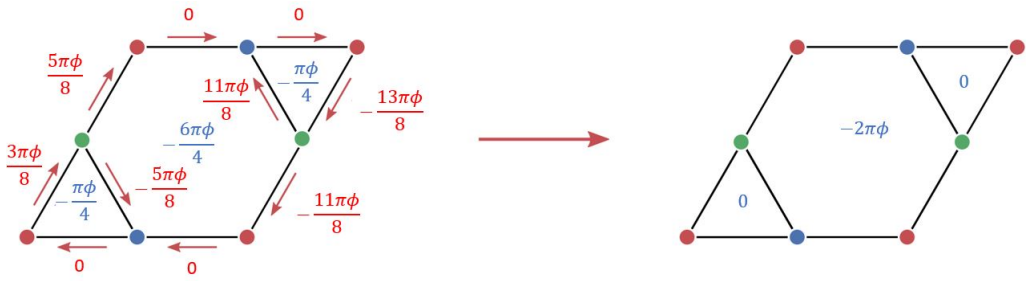

Figure 33: Redistribution of flux; (left) flux distribution under Maxwell field, (right) redistributed flux under Chern-Simons field.

The unit cell on the left-hand side of Figure (33) indicates the phases added to the hoppings by Peierl's substitution. As indicated in blue text the flux through each of the internal regions of the unit cell is non-zero. When CS field is present, however, the flux through the small triangular regions of the unit cell is completely withdrawn and added to the hexagonal region in the centre as it is shown on the right-hand side of the figure. This flux distribution can be achieved by assigning phases according to Figure (34).

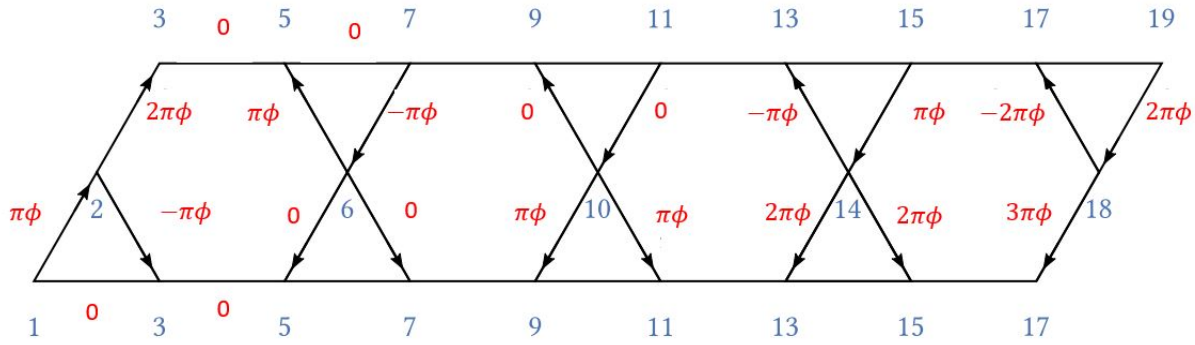

Figure 34: Flux phases with Chern-Simons field, red figures correspond to phases and blue to the values of m; flux through the triangular regions are made zero and all the flux goes through the hexagon in the centre of each unit cell.

After appropriately adding these phases to the Hamiltonian, the Hofstadter's spectrum can be plotted to show what happens to the flat band.

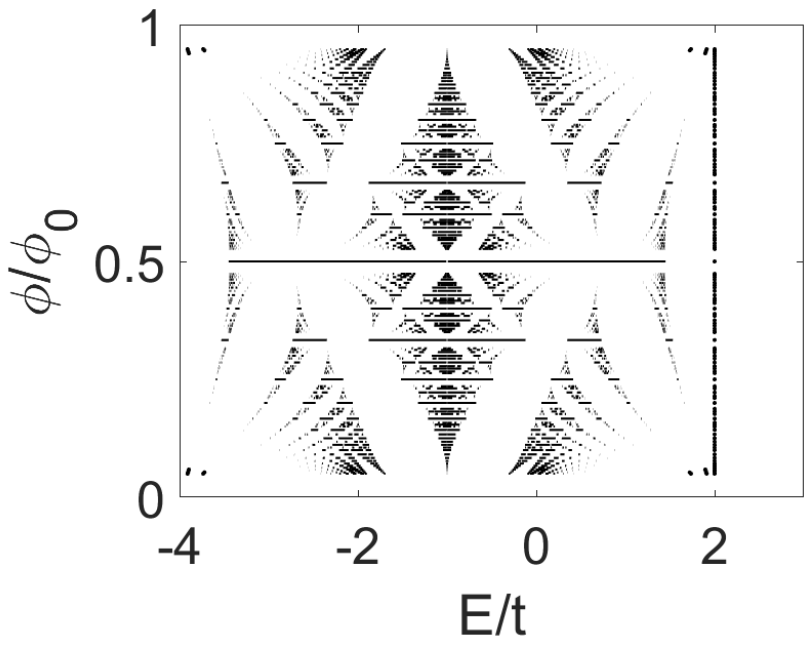

Figure 35: Hofstadter's spectrum of Kagome lattice in the presence of CS field; notice the flat band at $\frac{E}{t} = 2$, which is indicated by manually marked points. It shows that the flat band is preserved for all values of ϕ and also isolated.

Notice the vertical line at $\frac{E}{t} = 2$. Again, this was manually included by indicating with a dot whenever there is a band with zero width. The plot shows that the flat band is preserved for all values of ϕ and it is isolated.

6.2 CS Field on Lieb Lattice

Now, consider the Lieb lattice. The unit cell does not contain any internal structure as shown in Figure (36).

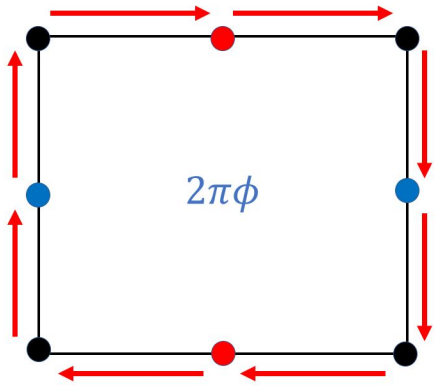

Figure 36: Flux through unit cell in Lieb lattice; Lieb lattice has no internal structure and thus the flux cannot be redistributed.

Hence, there cannot be redistribution of flux. In other words, applying CS field makes no difference from the Maxwell field. As it was seen in a previous chapter, with the Maxwell field, Lieb lattice preserved the isolated flat band. Thus, in both Kagome lattice and Lieb lattice, the presence of CS field imposes the protection of flat band while lifting the degeneracy.

6.3 Differentiating t_{inter} from t_{intra} in the presence of CS Field

It was shown previously that modifying the lattice by differentiating t_{inter} from t_{intra} introduced a family of Hamiltonian that preserved the flat band as well as the degeneracy. The goal of this section is to emphasize the effect of CS field on lattices, lifting degeneracy while preserving flat band. In particular, it will be tested if applying CS field on the modified Kagome lattice still preserves the flat band and lifts the degeneracy. This can be done very easily at this level by introducing coefficients $(1+r)$ and $(1-r)$ to the two kinds of hoppings in the Hamiltonian with the additional phases determined by the new flux distribution with the CS field. This time, instead of Hofstadter's spectrum, individual plots will be shown because each value of r, that controls t_{intra} and t_{inter}, gives a different spectrum.

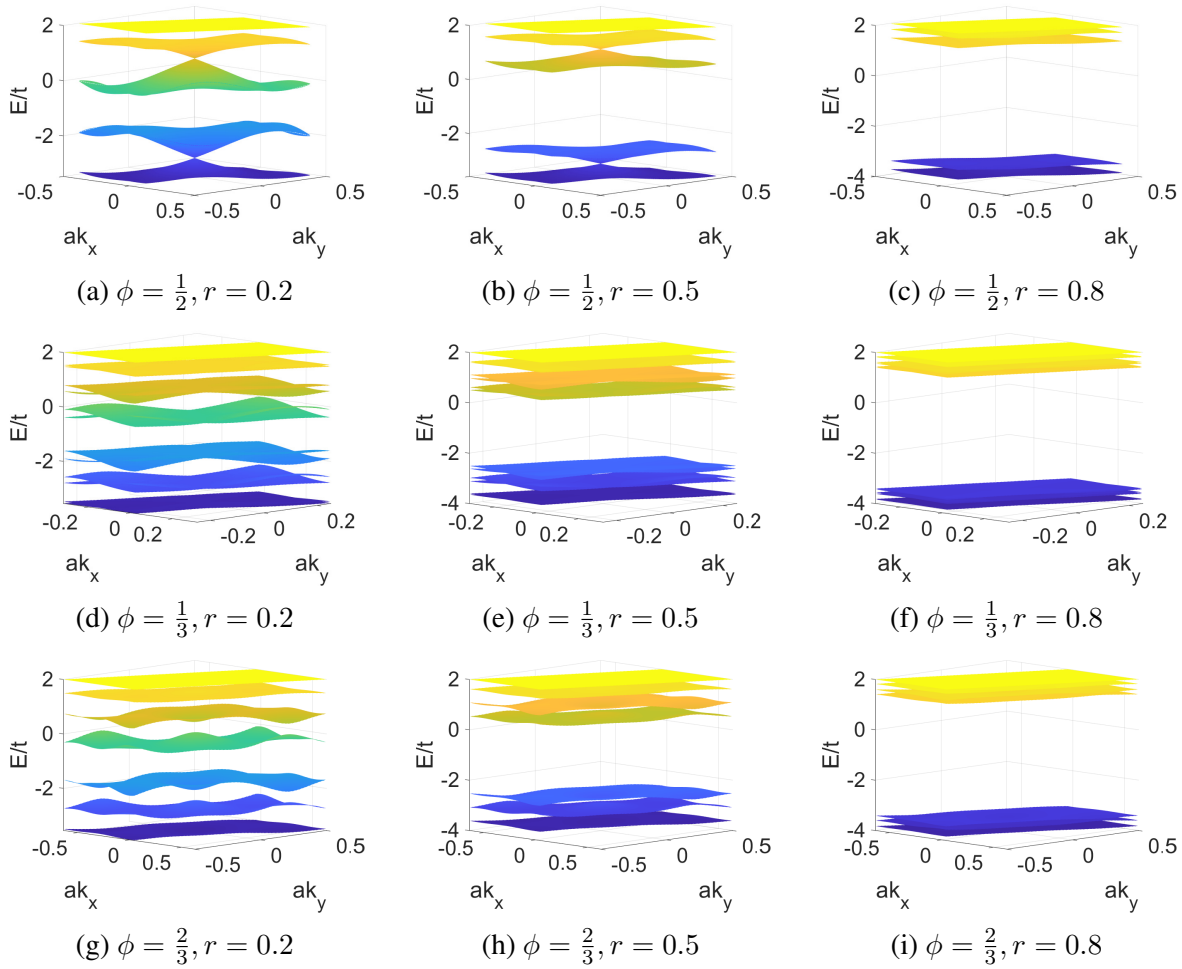

(a) $\phi = \frac{1}{2}, r = 0.2$ (b) $\phi = \frac{1}{2}, r = 0.5$ (c) $\phi = \frac{1}{2}, r = 0.8$

(d) $\phi = \frac{1}{3}, r = 0.2$ (e) $\phi = \frac{1}{3}, r = 0.5$ (f) $\phi = \frac{1}{3}, r = 0.8$

(g) $\phi = \frac{2}{3}, r = 0.2$ (h) $\phi = \frac{2}{3}, r = 0.5$ (i) $\phi = \frac{2}{3}, r = 0.8$

Figure 37: Energy dispersion of modified Kagome lattice in the presence of Chern-Simons field at various values of ϕ and r; notice that the flat band at $\frac{E}{t} = 2$ is protected and remains isolated.

The flat band at $\frac{E}{t} = 2$ is protected as predicted. The bands are divided in two groups where the upper group approaches the top flat band as r increases while the lower group approaches the bottom band. A similar pattern was observed with the modified Kagome lattice without the CS field.

6.4 Summary

In this chapter, it was demonstrated that the presence of CS field preserves and isolates flat bands. The effect of CS field at the level of unit cell is the redistribution of flux such that the flux is concentrated in one region when the unit cell has an internal structure. Since Kagome lattice has an internal structure, the flux distribution with magnetic field is different from that of CS field. Thus, the two outcomes are different in the sense that with the flux distribution of magnetic field the flat band became dispersive, while with that of CS field the flat band is

preserved. In the case of Lieb lattice, however, the absence of internal structure results in no distinction between magnetic field and CS field. Thus, even with magnetic field, the flat band is preserved.

7 Suggested Ideas for Further Study

Physical Interpretation of Mathematical Constraints for Degeneracy

The second method of calculating degeneracy in Chapter 5 is purely mathematical. This method can be further investigated to identify associated physical symmetries possibly by making a connection with the mathematical constraints presented. Having a physical interpretation may allow one to determine whether a system has degeneracy or not through simpler observation of the lattice structure instead of having to go through the calculations. This may also answer the question of why the modification of hopping amplitudes results in lifting the degeneracy in Lieb lattice while preserving that in Kagome lattice.

Study of Topology in Modified Kagome Lattice

Other interesting topics that can be further investigated are related to the modification of lattices by changing t_{intra} and t_{inter}. Notice in Figures (21) and (22) that as soon as r differs from zero, gap opens up between the two lower bands of the Kagome lattice, which corresponds to lifting the degeneracies at the K/K' points. It will be worthwhile to study the associated topology to examine whether the two phases, $r > 0$ and $r < 0$, are topologically distinct.
Moreover, as it was discussed in section 5.3.3, the middle band of Kagome lattice asymptotically approaches the flat band as $|r|$ approaches 1 and at $|r| = 1$ the two bands completely overlap with each other. This can be seen as the middle band penetrating through the flat band as $|r|$ changes around 1. It will be interesting to investigate if the associated topology changes when this incident occurs. Lastly, applying strains on the Kagome lattice caused the degeneracy of the flat band to split and relocate as it can be seen in Figure (15). It will be worthwhile to investigate the topology associated when this occurs.

Topology of Isolated Flat Bands

Studying the topology of a flat band necessarily requires the band to be gapped out. When it is coupled to a dispersive band like the case of the original Kagome lattice, the topology of the flat band cannot be identified. But now with the aid of CS field, the topology of isolated flat bands in the family of modified Kagome lattice (and Lieb lattice also) presented in section 5.3 can be investigated. In addition, since these systems exhibit correlation effects arising from the perfectly flat bands, they can provide suitable models for studying the FQHE.

Interplay Between Maxwell Field and CS Field

It is known that quantum Hall effect (QHE) is topological. Moreover, electronic interactions in QH systems, with flat bands, leads to emergence of CS field. The presence of CS field causes the formation of composite fermions and as a result, the system exhibits FQH states with topology of their own. Here, one can study the nature of the FQH state in a flat band system without magnetic field and also investigate what happens if magnetic field is applyed to the system.

8 Conclusion

Throughout the thesis Kagome lattice and Lieb lattice were studied because they both exhibit perfectly flat bands. In attempt to isolate the flat bands, applying an external magnetic field was considered. The Hofstadter's spectrum revealed that the degeneracy of the flat band in Kagome lattice was indeed lifted but at the same time the flat band was no longer flat, it became dispersive. This consequently demonstrated that breaking TRS is not sufficient to isolate the flat band in Kagome lattice.

Then, to study the robustness of flat band, three kinds of (realizable) modifications to the lattice were considered. The first two were applying strains along the two diagonal axes of the unit cell and making the three types of atoms in the lattice different from one another. Both resulted in making the flat band dispersive. The third kind of modification grouped the hopping amplitudes into two; hoppings within the unit cell, defined as t_{intra}, and hoppings between the unit cells, defined as t_{inter}, then it varied the ratio of t_{intra} and t_{inter}. It was shown that for any value of this ratio, the flat band is preserved. This provided a family of perfectly flat band systems.

Returning to the discussion of lifting degeneracy and isolating flat band, CS field was introduced. The difference between CS field and magnetic field on the lattice was the distribution of flux in the unit cell. While the flux due to magnetic field was spread throughout all three regions bounded by the bonds inside the unit cell, the flux due to CS field was concentrated in one region such that the other two regions had zero flux. The Hofstadter's spectrum based on the CS flux distribution demonstrated that the flat band is preserved and the degeneracy is lifted for all possible values of flux per unit cell.

On the other hand, it was observed that applying a magnetic field successfully isolates the flat band of Lieb lattice. The Hofstadter's spectrum showed that the flat band remains flat under the presence of magnetic field. At the same time, it also showed that the flat band gets gapped out as soon as magnetic field is applied. The different result from the Kagome lattice is due to the fact that the Lieb lattice has no internal structure in the unit cell. The absence of internal structure allows the flux to be distributed in a unique way, which makes the effects of magnetic field and CS field the same.

It is worthwhile to note that the emergence of CS field is a consequence of electronic interaction in flat bands. Other phenomena such as unconventional superconductivity, Mott insulator, and Wigner crystal also arise due to strong electronic interaction in flat bands. The scope of this thesis was not focused on studying these specific phenomena but exploring how to make the basic ingredient, the flat band systems, available for the desired studies.

The same modification that produced a family of Kagome lattice (varying the ratio between

t_{intra} and t_{inter}) was also applied to the Lieb lattice. It was shown that the flat band is preserved also for the Lieb lattice, which implied that another family of flat band systems was introduced.

While studying the degeneracy of the two lattices, a method of calculating degeneracy without requiring the calculation of eigenvalues was introduced. By finding the appropriate constraints to the Hamiltonians, the degeneracies in Kagome lattice and Lieb lattice as well as Graphene and extended square lattice were calculated.

Furthermore, a few ideas for further research were proposed. One is connecting the mathematical constraints discussed for calculating degeneracy with physical symmetries. Another is comparing the topology of modified Kagome lattice when the inter-unit cell hopping amplitudes are greater than the intra-unit cell hopping amplitudes with the opposite case. In addition, when either the inter-unit cell or the intra-unit cell hopping amplitudes become negative, it can be examined if the topology changes. Last suggestion is studying the topology of flat bands that are isolated by the help of CS field.

Overall, two results can be emphasized. It was demonstrated that breaking TRS is not sufficient to isolate and preserve the flat band in Kagome lattice. Instead, it required CS field to successfully isolate the flat band. Furthermore, it was demonstrated that there is a family of flat band systems. They are realizable as they involve short-range hoppings.

9 Appendix

Proof of $\sum_{n=1}^{3} |\cos(\frac{kR_n}{2} - i\frac{\alpha}{2})|^2 = \sum_{n=1}^{3} \cos^2(\frac{kR_n}{2}) + 3sinh^2(\frac{\alpha}{2})$

$$\sum_{n=1}^{3} |\cos(\frac{kR_n}{2} - i\frac{\alpha}{2})|^2$$

$$= \sum_{n=1}^{3} |\cos(\frac{kR_n}{2})\cos(i\frac{\alpha}{2}) + sin(\frac{kR_n}{2})sin(i\frac{\alpha}{2})|^2$$

$$= \sum_{n=1}^{3} [\cos(\frac{kR_n}{2})\cos(i\frac{\alpha}{2}) + sin(\frac{kR_n}{2})sin(i\frac{\alpha}{2})][\cos(\frac{kR_n}{2})\cos(i\frac{\alpha}{2}) - sin(\frac{kR_n}{2})sin(i\frac{\alpha}{2})]$$

$$= \sum_{n=1}^{3} [\cos^2(\frac{kR_n}{2})\cos^2(i\frac{\alpha}{2}) - sin^2(\frac{kR_n}{2})sin^2(i\frac{\alpha}{2})]$$

$$= \sum_{n=1}^{3} [\cos^2(\frac{kR_n}{2})cosh^2(\frac{\alpha}{2}) + sin^2(\frac{kR_n}{2})sinh^2(\frac{\alpha}{2})]$$

$$= \sum_{n=1}^{3} [\cos^2(\frac{kR_n}{2}) + \cos^2(\frac{kR_n}{2})sinh^2(\frac{\alpha}{2}) + sin^2(\frac{kR_n}{2})sinh^2(\frac{\alpha}{2})]$$

$$= \sum_{n=1}^{3} \cos^2(\frac{kR_n}{2}) + 3sinh^2(\frac{\alpha}{2})$$

Proof of $2Re[\prod_{n=1}^{3}\cos(\frac{kR_n}{2}(-1)^{n+1}i\frac{\alpha}{2})]$
$= 2cosh(\frac{\alpha}{2})\prod_{n=1}^{3}\cos(\frac{kR_n}{2}) + 2cosh(\frac{\alpha}{2})sinh^2(\frac{\alpha}{2})$

$$2Re[\prod_{n=1}^{3}\cos(\frac{kR_n}{2}(-1)^{n+1}i\frac{\alpha}{2})]$$

$$= \frac{1}{2}Re[\cos(\frac{kR_1}{2} - \frac{kR_2}{2} - \frac{kR_3}{2} + i\frac{\alpha}{2}) + \cos(\frac{kR_1}{2} - \frac{kR_2}{2} + \frac{kR_3}{2} + 3i\frac{\alpha}{2}) + \cos(\frac{kR_1}{2} + \frac{kR_2}{2} - \frac{kR_3}{2} - i\frac{\alpha}{2}) + \cos(\frac{kR_1}{2} + \frac{kR_2}{2} + \frac{kR_3}{2} + i\frac{\alpha}{2})]$$

$$= \frac{1}{2}Re[\cos(kR_3 - i\frac{\alpha}{2}) + \cos(3i\frac{\alpha}{2}) + \cos(kR_1 - i\frac{\alpha}{2}) + \cos(kR_2 + i\frac{\alpha}{2})]$$

$$= \frac{1}{2}Re[\cos(kR_1)\cos(i\frac{\alpha}{2}) + sin(kR_1)sin(i\frac{\alpha}{2}) + \cos(kR_2)\cos(i\frac{\alpha}{2}) - sin(kR_2)sin(i\frac{\alpha}{2}) + \cos(kR_3)\cos(i\frac{\alpha}{2}) + sin(kR_3)sin(i\frac{\alpha}{2}) + \cos(2i\frac{\alpha}{2})\cos(i\frac{\alpha}{2}) - sin(2i\frac{\alpha}{2})sin(i\frac{\alpha}{2})]$$

$$= \frac{1}{2}[\cos(kR_3 - i\frac{\alpha}{2}) + \cos(3i\frac{\alpha}{2}) + \cos(kR_1 - i\frac{\alpha}{2}) + \cos(kR_2 + i\frac{\alpha}{2})]$$

$$= \frac{1}{2}[\cos(kR_1)\cos(i\frac{\alpha}{2}) + \cos(kR_2)\cos(i\frac{\alpha}{2}) + \cos(kR_3)\cos(i\frac{\alpha}{2}) + \cos(2i\frac{\alpha}{2})\cos(i\frac{\alpha}{2}) - sin(2i\frac{\alpha}{2})sin(i\frac{\alpha}{2})]$$

$$= \frac{1}{2}[\cos(i\frac{\alpha}{2})\{\cos(kR_1) + \cos(kR_2) + \cos(kR_3)\} + \cos(i\frac{\alpha}{2})\{1 - 2sin^2(i\frac{\alpha}{2})\} - 2sin^2(i\frac{\alpha}{2})\cos(i\frac{\alpha}{2})]$$

$$= \frac{1}{2}[\cos(i\frac{\alpha}{2})\{2\cos(\frac{kR_1 + kR_3}{2})\cos(\frac{kR_1 - kR_3}{2}) + \cos(kR_2)\} + \cos(i\frac{\alpha}{2}) - 2\cos(i\frac{\alpha}{2})sin^2(i\frac{\alpha}{2}) - 2sin^2(i\frac{\alpha}{2})\cos(i\frac{\alpha}{2})]$$

$$= \frac{1}{2}[cosh(\frac{\alpha}{2})\{2\cos(\frac{kR_2}{2})\cos(\frac{kR_1 - kR_3}{2}) + \cos(kR_2)\} + cosh(\frac{\alpha}{2}) - 4cosh(\frac{\alpha}{2})sin^2(\frac{\alpha}{2})]$$

$$= \frac{1}{2}[cosh(\frac{\alpha}{2})\{2\cos(\frac{kR_2}{2})\cos(\frac{kR_1 - kR_3}{2})$$

$$= \frac{1}{2}[cosh(\frac{\alpha}{2})\{2\cos(\frac{kR_2}{2})[\cos(\frac{kR_1 - kR_3}{2}) + \cos(\frac{kR_2}{2})] - 1\} + cosh(\frac{\alpha}{2}) - 4cosh(\frac{\alpha}{2})sin^2(\frac{\alpha}{2})]$$

$$= \frac{1}{2}[cosh(\frac{\alpha}{2})\{4\cos(\frac{kR_2}{2})\cos(\frac{kR_1 - kR_3 + kR_2}{4})\cos(\frac{kR_1 - kR_3 - kR_2}{4}) - 1\} + cosh(\frac{\alpha}{2}) - 4cosh(\frac{\alpha}{2})sin^2(\frac{\alpha}{2})]$$

$$= \frac{1}{2}[cosh(\frac{\alpha}{2})\{4\cos(\frac{kR_2}{2})\cos(\frac{kR_1}{2})\cos(\frac{kR_3}{2}) - 1\} + cosh(\frac{\alpha}{2}) - 4cosh(\frac{\alpha}{2})sin^2(\frac{\alpha}{2})]$$

$$= \frac{1}{2}[cosh(\frac{\alpha}{2})4\cos(\frac{kR_2}{2})\cos(\frac{kR_1}{2})\cos(\frac{kR_3}{2}) - 4cosh(\frac{\alpha}{2})sin^2(\frac{\alpha}{2})]$$

$$= 2cosh(\frac{\alpha}{2})\prod_{n=1}^{3}\cos(\frac{kR_n}{2}) + 2cosh(\frac{\alpha}{2})sinh^2(\frac{\alpha}{2})$$

Proof of $\sum_{n=1}^{3} |sin(\frac{kR_n}{2} - i\frac{\alpha}{2})|^2 = -\sum_{n=1}^{3} \cos^2(\frac{kR_n}{2}) + 3cosh^2(\frac{\alpha}{2})$

$$\sum_{n=1}^{3} |sin(\frac{kR_n}{2} - i\frac{\alpha}{2})|^2$$

$$= \sum_{n=1}^{3} |sin(\frac{kR_n}{2})\cos(i\frac{\alpha}{2}) - \cos(\frac{kR_n}{2})sin(i\frac{\alpha}{2})|^2$$

$$= \sum_{n=1}^{3} [sin(\frac{kR_n}{2})cosh(\frac{\alpha}{2}) - i\cos(\frac{kR_n}{2})sinh(\frac{\alpha}{2})][sin(\frac{kR_n}{2})cosh(\frac{\alpha}{2}) + i\cos(\frac{kR_n}{2})sinh(\frac{\alpha}{2})]$$

$$= \sum_{n=1}^{3} [sin^2(\frac{kR_n}{2})cosh^2(\frac{\alpha}{2}) + \cos^2(\frac{kR_n}{2})sinh^2(\frac{\alpha}{2})]$$

$$= \sum_{n=1}^{3} [cosh^2(\frac{\alpha}{2}) - \cos^2(\frac{kR_n}{2})cosh^2(\frac{\alpha}{2}) + \cos^2(\frac{kR_n}{2})cosh^2(\frac{\alpha}{2}) - \cos^2(\frac{kR_n}{2})]$$

$$= \sum_{n=1}^{3} [cosh^2(\frac{\alpha}{2}) - \cos^2(\frac{kR_n}{2})]$$

$$= -\sum_{n=1}^{3} \cos^2(\frac{kR_n}{2}) + 3cosh^2(\frac{\alpha}{2})$$

References

[1] E. Tang, J.-W. Mei, and X.-G. Wen, "High-Temperature Fractional Quantum Hall States," en, *Physical Review Letters*, vol. 106, no. 23, p. 236 802, Jun. 2011, ISSN: 0031-9007, 1079-7114. DOI: 10.1103/PhysRevLett.106.236802. [Online]. Available: https://link.aps.org/doi/10.1103/PhysRevLett.106.236802 (visited on 08/27/2020).

[2] Y.-F. Wang, Z.-C. Gu, C.-D. Gong, and D. N. Sheng, "Fractional Quantum Hall Effect of Hard-Core Bosons in Topological Flat Bands," en, *Physical Review Letters*, vol. 107, no. 14, p. 146 803, Sep. 2011, arXiv: 1103.1686, ISSN: 0031-9007, 1079-7114. DOI: 10.1103/PhysRevLett.107.146803. [Online]. Available: http://arxiv.org/abs/1103.1686 (visited on 10/31/2020).

[3] B. Jaworowski, "Wigner crystallization in topological flat bands," en, *New J. Phys.*, p. 21, 2018.

[4] Z. Liu, F. Liu, and Y.-S. Wu, "Exotic electronic states in the world of flat bands: From theory to material," en, *Chinese Physics B*, vol. 23, no. 7, p. 077 308, Jul. 2014, ISSN: 1674-1056. DOI: 10.1088/1674-1056/23/7/077308. [Online]. Available: https://iopscience.iop.org/article/10.1088/1674-1056/23/7/077308 (visited on 12/09/2020).

[5] C. Wu, D. Bergman, L. Balents, and S. Das Sarma, "Flat Bands and Wigner Crystallization in the Honeycomb Optical Lattice," en, *Physical Review Letters*, vol. 99, no. 7, p. 070 401, Aug. 2007, ISSN: 0031-9007, 1079-7114. DOI: 10.1103/PhysRevLett.99.070401. [Online]. Available: https://link.aps.org/doi/10.1103/PhysRevLett.99.070401 (visited on 12/09/2020).

[6] Y. Cao, V. Fatemi, S. Fang, K. Watanabe, T. Taniguchi, E. Kaxiras, and P. Jarillo-Herrero, "Unconventional superconductivity in magic-angle graphene superlattices," en, *Nature*, vol. 556, no. 7699, pp. 43–50, Apr. 2018, ISSN: 0028-0836, 1476-4687. DOI: 10.1038/nature26160. [Online]. Available: http://www.nature.com/articles/nature26160 (visited on 08/27/2020).

[7] L. Balents, C. R. Dean, D. K. Efetov, and A. F. Young, "Superconductivity and strong correlations in moiré flat bands," en, *Nature Physics*, vol. 16, no. 7, pp. 725–733, Jul. 2020, ISSN: 1745-2473, 1745-2481. DOI: 10.1038/s41567-020-0906-9. [Online]. Available: http://www.nature.com/articles/s41567-020-0906-9 (visited on 08/27/2020).

[8] Y. Cao, V. Fatemi, A. Demir, S. Fang, S. L. Tomarken, J. Y. Luo, J. D. Sanchez-Yamagishi, K. Watanabe, T. Taniguchi, E. Kaxiras, R. C. Ashoori, and P. Jarillo-Herrero, "Correlated insulator behaviour at half-filling in magic-angle graphene superlattices," en, *Nature*, vol. 556, no. 7699, pp. 80–84, Apr. 2018, ISSN: 0028-0836, 1476-4687. DOI: 10.1038/nature26154. [Online]. Available: http://www.nature.com/articles/nature26154 (visited on 08/27/2020).

[9] A. Dauphin, M. Müller, and M. A. Martin-Delgado, "Quantum simulation of a topological Mott insulator with Rydberg atoms in a Lieb lattice," en, *Physical Review A*, vol. 93, no. 4, p. 043 611, Apr. 2016, ISSN: 2469-9926, 2469-9934. DOI: 10.1103/PhysRevA.93.043611. [Online]. Available: https://link.aps.org/doi/10.1103/PhysRevA.93.043611 (visited on 10/31/2020).

[10] N. R. Chebrolu, B. L. Chittari, and J. Jung, "Flat bands in twisted double bilayer graphene," en, *Physical Review B*, vol. 99, no. 23, p. 235 417, Jun. 2019, ISSN: 2469-9950, 2469-9969. DOI: 10.1103/PhysRevB.99.235417. [Online]. Available: https://link.aps.org/doi/10.1103/PhysRevB.99.235417 (visited on 10/17/2020).

[11] K. Kim, A. DaSilva, S. Huang, B. Fallahazad, S. Larentis, T. Taniguchi, K. Watanabe, B. J. LeRoy, A. H. MacDonald, and E. Tutuc, "Tunable moiré bands and strong correlations in small-twist-angle bilayer graphene," en, *Proceedings of the National Academy of Sciences*, vol. 114, no. 13, pp. 3364–3369, Mar. 2017, ISSN: 0027-8424, 1091-6490. DOI: 10.1073/pnas.1620140114. [Online]. Available: http://www.pnas.org/lookup/doi/10.1073/pnas.1620140114 (visited on 11/01/2020).

[12] M. Yankowitz, S. Chen, H. Polshyn, Y. Zhang, K. Watanabe, T. Taniguchi, D. Graf, A. F. Young, and C. R. Dean, "Tuning superconductivity in twisted bilayer graphene," en, *Science*, vol. 363, no. 6431, pp. 1059–1064, Mar. 2019, ISSN: 0036-8075, 1095-9203. DOI: 10.1126/science.aav1910. [Online]. Available: https://www.sciencemag.org/lookup/doi/10.1126/science.aav1910 (visited on 11/01/2020).

[13] X. Lu, P. Stepanov, W. Yang, M. Xie, M. A. Aamir, I. Das, C. Urgell, K. Watanabe, T. Taniguchi, G. Zhang, A. Bachtold, A. H. MacDonald, and D. K. Efetov, "Superconductors, orbital magnets and correlated states in magic-angle bilayer graphene," en, *Nature*, vol. 574, no. 7780, pp. 653–657, Oct. 2019, ISSN: 0028-0836, 1476-4687. DOI: 10.1038/s41586-019-1695-0. [Online]. Available: http://www.nature.com/articles/s41586-019-1695-0 (visited on 11/01/2020).

[14] M. Fidrysiak, M. Zegrodnik, and J. Spałek, "Unconventional topological superconductivity and phase diagram for an effective two-orbital model as applied to twisted bilayer graphene," en, *Physical Review B*, vol. 98, no. 8, p. 085 436, Aug. 2018, ISSN: 2469-9950, 2469-9969. DOI: 10.1103/PhysRevB.98.085436. [Online]. Available: https://link.aps.org/doi/10.1103/PhysRevB.98.085436 (visited on 10/17/2020).

[15] Y. Xu and H. Pu, "Building Flat-Band Lattice Models from Gram Matrices," en, *arXiv:2002.06767 [cond-mat]*, Sep. 2020, arXiv: 2002.06767. [Online]. Available: http://arxiv.org/abs/2002.06767 (visited on 10/24/2020).

[16] D. L. Bergman, C. Wu, and L. Balents, "Band touching from real-space topology in frustrated hopping models," en, *Physical Review B*, vol. 78, no. 12, p. 125 104, Sep. 2008, ISSN: 1098-0121, 1550-235X. DOI: 10.1103/PhysRevB.78.125104. [Online]. Available: https://link.aps.org/doi/10.1103/PhysRevB.78.125104 (visited on 08/27/2020).

[17] D. Green, L. Santos, and C. Chamon, "Isolated Flat Bands and Spin-1 Conical Bands in Two-Dimensional Lattices," en, *Physical Review B*, vol. 82, no. 7, p. 075 104, Aug. 2010, arXiv: 1004.0708, ISSN: 1098-0121, 1550-235X. DOI: 10.1103/PhysRevB.82.075104. [Online]. Available: http://arxiv.org/abs/1004.0708 (visited on 08/27/2020).

[18] Y. Zhou, K. Kanoda, and T.-K. Ng, "Quantum spin liquid states," en, *Reviews of Modern Physics*, vol. 89, no. 2, p. 025 003, Apr. 2017, ISSN: 0034-6861, 1539-0756. DOI: 10.1103/RevModPhys.89.025003. [Online]. Available: http://link.aps.org/doi/10.1103/RevModPhys.89.025003 (visited on 10/31/2020).

[19] T.-H. Han, J. S. Helton, S. Chu, D. G. Nocera, J. A. Rodriguez-Rivera, C. Broholm, and Y. S. Lee, "Fractionalized excitations in the spin-liquid state of a kagome-lattice antiferromagnet," en, *Nature*, vol. 492, no. 7429, pp. 406–410, Dec. 2012, ISSN: 0028-0836, 1476-4687. DOI: 10.1038/nature11659. [Online]. Available: http://www.nature.com/articles/nature11659 (visited on 10/31/2020).

[20] L. Ye, M. Kang, J. Liu, F. von Cube, C. R. Wicker, T. Suzuki, C. Jozwiak, A. Bostwick, E. Rotenberg, D. C. Bell, L. Fu, R. Comin, and J. G. Checkelsky, "Massive Dirac fermions in a ferromagnetic kagome metal," en, *Nature*, vol. 555, no. 7698, pp. 638–642, Mar. 2018, ISSN: 0028-0836, 1476-4687. DOI: 10.1038/nature25987. [Online]. Available: http://www.nature.com/articles/nature25987 (visited on 10/31/2020).

[21] A. Julku, S. Peotta, T. I. Vanhala, D.-H. Kim, and P. Törmä, "Geometric Origin of Superfluidity in the Lieb-Lattice Flat Band," en, *Physical Review Letters*, vol. 117, no. 4, p. 045 303, Jul. 2016, ISSN: 0031-9007, 1079-7114. DOI: 10.1103/PhysRevLett.117.045303. [Online]. Available: https://link.aps.org/doi/10.1103/PhysRevLett.117.045303 (visited on 10/31/2020).

[22] H. Tamura, K. Shiraishi, T. Kimura, and H. Takayanagi, "Flat-band ferromagnetism in quantum dot superlattices," en, *Physical Review B*, vol. 65, no. 8, p. 085 324, Feb. 2002, ISSN: 0163-1829, 1095-3795. DOI: 10.1103/PhysRevB.65.085324. [Online]. Available: https://link.aps.org/doi/10.1103/PhysRevB.65.085324 (visited on 10/31/2020).

[23] S. Taie, H. Ozawa, T. Ichinose, T. Nishio, S. Nakajima, and Y. Takahashi, "Coherent driving and freezing of bosonic matter wave in an optical Lieb lattice," en, *arXiv:1506.00587 [cond-mat]*, Nov. 2015, arXiv: 1506.00587. DOI: 10.1126/sciadv.1500854. [Online]. Available: http://arxiv.org/abs/1506.00587 (visited on 11/26/2020).

[24] W. Jiang, H. Huang, and F. Liu, "A Lieb-like lattice in a covalent-organic framework and its Stoner ferromagnetism," en, *Nature Communications*, vol. 10, no. 1, p. 2207, Dec. 2019, ISSN: 2041-1723. DOI: 10.1038/s41467-019-10094-3. [Online]. Available: http://www.nature.com/articles/s41467-019-10094-3 (visited on 10/31/2020).

[25] B. Cui, X. Zheng, J. Wang, D. Liu, S. Xie, and B. Huang, "Realization of Lieb lattice in covalent-organic frameworks with tunable topology and magnetism," en, *Nature Communications*, vol. 11, no. 1, p. 66, Dec. 2020, ISSN: 2041-1723. DOI: 10.1038/s41467-019-13794-y. [Online]. Available: http://www.nature.com/articles/s41467-019-13794-y (visited on 10/31/2020).

[26] L. Du, Q. Chen, A. D. Barr, A. R. Barr, and G. A. Fiete, "Floquet Hofstadter butterfly on the kagome and triangular lattices," en, *Physical Review B*, vol. 98, no. 24, p. 245 145, Dec. 2018, ISSN: 2469-9950, 2469-9969. DOI: 10.1103/PhysRevB.98.245145. [Online]. Available: https://link.aps.org/doi/10.1103/PhysRevB.98.245145 (visited on 11/22/2020).

[27] F. Yılmaz, F. N. Ünal, and M. Ö. Oktel, "Evolution of the Hofstadter butterfly in a tunable optical lattice," en, *Physical Review A*, vol. 91, no. 6, p. 063 628, Jun. 2015, ISSN: 1050-2947, 1094-1622. DOI: 10.1103/PhysRevA.91.063628. [Online]. Available: https://link.aps.org/doi/10.1103/PhysRevA.91.063628 (visited on 11/22/2020).

[28] G. V. Dunne, "Aspects Of Chern-Simons Theory," en, in *Aspects topologiques de la physique en basse dimension. Topological aspects of low dimensional systems*, A. Comtet, T. Jolicœur, S. Ouvry, and F. David, Eds., vol. 69, Series Title: Les Houches - Ecole d'Ete de Physique Theorique, Berlin, Heidelberg: Springer Berlin Heidelberg, 1999, pp. 177–263, ISBN: 978-3-540-66909-8. DOI: 10.1007/3-540-46637-1_3. [Online]. Available: http://link.springer.com/10.1007/3-540-46637-1_3 (visited on 11/22/2020).

[29] S. Maiti and T. Sedrakyan, "Fermionization of bosons in a flat band," en, *Physical Review B*, vol. 99, no. 17, p. 174 418, May 2019, ISSN: 2469-9950, 2469-9969. DOI: 10.1103/PhysRevB.99.174418. [Online]. Available: https://link.aps.org/doi/10.1103/PhysRevB.99.174418 (visited on 11/22/2020).